University of Wisconsin - Madison

MAD/PH/359
July 1987

Experimental Challenges to the Standard Model: A Re-evaluation.

Ph. D. Thesis

J.R. CUDELL

*Physics Department, University of Wisconsin, Madison, Wisconsin 53706**

ABSTRACT

We re-examine data that seem at first sight to contradict the 'Standard Model' of weak, electromagnetic and strong interactions. We concentrate on experiments for which the use of perturbative methods is legitimate.

We show that the monojet signal observed at the CERN $p\bar{p}$ collider is consistent with standard perturbative estimates after background subtraction.

Charm hadroproduction can be considered a measurement of the charm current mass and using the LEBC EHS and LEBC SPS data we obtain a value consistent with other current estimates.

We then consider same-sign-dilepton production, where we carefully evaluate all the theoretical uncertainties. The most recent CDHS data are marginally consistent with our highest estimate.

We then turn to the Cygnus X-3 puzzle and review the main properties of the system and the main calculational results. We conclude here that the Standard Model or its extensions totally fail to accomodate the data on muons from point sources.

* Permanent address from October 1987: *DAMTP, University of Cambridge, Silver Street, Cambridge CB3 9EW, United Kingdom*

ACKNOWLEDGMENTS

I would like to thank all the persons who made my research possible. First and above all, I wish to thank my advisor, Professor Francis Halzen for his constant support, for the numerous insights he let me share with him and for the physical intuition he helped me develop. I also want to thank Dr. Ken-Ichi Hikasa and Professor Paul Hoyer for our fruitful collaborations.

I am also grateful to Professor Vernon Barger, Professor Charles Goebel, Professor Thomas K. Gaisser, Professor Todor Stanev and Dr. Xerxes Tata who have always been available for discussion and whose suggestions have been of great help. Many thanks also to William F. Long for sharing his vast computer knowledge with me.

I further want to mention here my fellow graduate students Dr. Cahit Erkal, Dr. Friedrich Olness, William Putikka, Kim Simmons and Jeffrey Schmidt for constantly exchanging ideas with me.

Finally, I am particularly grateful to Carmen Ana Pont for proof reading the manuscript and for her many encouragements during these years of research.

This research was supported in part by the University of Wisconsin Research Committee with funds granted by the Wisconsin Alumni Research Foundation, and in part by the U. S. Department of Energy under contract DE-AC02-76ER00881.

Table of Contents

Introduction

The so-called 'Standard Model' of the weak, electromagnetic and strong interactions based on the gauge symmetry $SU(3)_c \otimes SU(2)_L \otimes U(1)$ and developed ten years ago is up to now extremely successful. This fact is extremely unsatisfactory on the theoretical side due to the large number of parameters left undetermined (18 in the minimal version of the model) and of fundamental questions left unanswered (*e.g.* the number of generations, the quantization of gravity...).

On the experimental side, a few results seem at first sight in contradiction with its predictions. These come from all regions of high-energy physics. Too many monojets seem to be produced at CERN, too many charmed particles in πp and pp beam-dump experiments, too many same-sign dileptons in νp beam-dump experiments and too many muons are seen in deep-underground detectors and in surface arrays in the direction of Cygnus X-3. In this thesis, I shall re-examine these data and compare them with the minimal Standard Model.

This work can be divided in two parts, depending on the level of disagreement between theory and experiment.

- First of all , QCD perturbative field theory has only a limited range of validity. This means that the predictions of hadronic physics are subject to numerous uncertainties. Careful evaluation of these show that the CERN 'anomalous' events, charm hadroproduction and same-sign-dilepton production in νp collisions can be made marginally consistent with the Standard Model. Extraction of new physics signals from these should prove very difficult due to these uncertainties.
- One is then left with the puzzle of Cygnus X-3. We shall show not only that the Standard Model cannot explain the observed results, but also that no proposed extension of the Standard Model can.

CHAPTER 1

The CERN Monojets

1.1 Data and Statement of the Problem

The CERN $p\bar{p}$ collider has been designed to observe the weak intermediate bosons. The observation of events with large missing transverse energy is the crucial tool used for this discovery. It provides the sample of $W \to e\nu$ decays but also additional events in which the missing transverse energy recoils against one jet. This is what one calls monojets![1-4]

The events are selected according to several criteria[1]:

1. cuts on the transverse energy of the electromagnetic calorimeters, or of the jet, or on the missing transverse energy $\not\!\!E_T$;
2. observation of at least one jet as defined by the UA1 algorithm[1] with $\Delta R = 0.4$, limitation to the 4σ sample (*i.e.* $\not\!\!E_T/0.7\sqrt{\Sigma E_T} \geq 4$);
3. isolation and veto cuts to minimize the jet fluctuations and the light-leptons background.

After combining the 546 GeV (118 nb^{-1}) run with the 630 GeV (597 nb^{-1}), 56 events survive these cuts. Among them, 3.8 are expected to come from jet fluctuations and 3.6 from W decay into light leptons. Half of the remaining events come from $W \to \tau\nu$; $\tau \to hadrons + \nu$. One can separate these using the method of τ-log-likelihood, which from the results of a Monte-Carlo study and from measuring the jet thickness, the direction of the leading

particle and the charged-particle multiplicity, can reject 78% of the $\tau \to hadrons + \nu$ events and isolate 89 % of the remaining events.

One is then left with 24 events. Among these, 17 have a jet transverse energy smaller than 40 GeV and are explained by $W \to lepton + \nu$ decays (1.4 events), $W \to \tau\nu$ and $W \to \nu\bar{\nu}$ (7.1 events), jet fluctuations (3.4 events) and $Z^0 \to \nu\bar{\nu}$ (5.6 events). Four additional events can be gotten from $W \to t\bar{b}$ and $Z^0 \to t\bar{t}$, $W \to t\bar{b}, \bar{t}b$ if the mass of the top quark is 30 GeV.

One has thus reduced the sample to 7 (or 3) events with high missing transverse energy ($\geq$ 40 GeV). The main standard-model source for such events is the Z^0 decay into neutrinos. Thus a careful evaluation of this process is required to see if that signal can contain any new physics. At the same time, we shall recalculate this background for lower-E_T jets.

1.2 The Drell-Yan Mechanism

General Features Monojets can occur in the standard model as a result of the production of weak bosons in association with gluons: $Z^0(\to \nu\bar{\nu}) + gluons$. Not only the event structure but also the kinematic features of monojets can be mimicked. As a function of the jet transverse momentum p_T the monojet cross section shows the usual QCD-type falloff at large p_T as well as a sharp cutoff at low p_T (typically $p_T \leq 30$ GeV) because of detection efficiency. A $Z^0 \to \nu\bar{\nu}$ decay is indeed unobservable at $p_T = 0$ (as there is no transverse-momentum imbalance) and the detector reaches a 90% efficiency for $p_T \approx 35$ GeV. As a kinematic reflection, the jet invariant mass also rises sharply in the 110–120 GeV region; at larger p_T values it again displays the

familiar QCD suppression. Notice that 'monojets' is a misnomer given that for large p_T values two or three jets are almost as likely to balance the Z^0 transverse momentum as a single jet. This is clearly illustrated by existing $Z^0 \to l\bar{l}$ data[5] and is certainly expected from a theoretical point of view. A completely parallel discussion can be made for $l + \not{p}_T + jet$ events[2,3] with $W \to l\nu$ substituted for $Z^0 \to \nu\bar{\nu}$. The uncertainty in the evaluation of this standard-model background has two main sources:

- ambiguities in the perturbative calculation of weak-boson yields as a function of their transverse momentum;
- dependence of the branching ratio $B(Z^0 \to \nu\bar{\nu})$ on the unknown but constrained[6,7,8] number of light neutrinos.

We shall now concentrate on the perturbative uncertainties.

Accuracy of Perturbative QCD

From a theoretical point of view, there are two distinct regimes for producing weak bosons: $p_T \ll M_Z$ and $p_T \approx M_Z$. Calculations exist covering both kinematic regions.[9,10] Calculations in the $p_T \ll M_Z$ region require the resummation of the gluon emission and are at best exploratory. Independently of any theoretical question, they are based on 'leading-logarithm kinematics' where one routinely computes momentum fractions of the partons as $x = M_Z/\sqrt{s}$ whereas exact kinematics dictates $x = (M_Z + p_T)/\sqrt{s}$ at y=0. Even at $p_T = 15$ GeV this leads to ambiguities of the order of a factor 2 in evaluating the parton flux factor $q(x_1)q(x_2)$.

At $p_T \approx M_Z$ the cross sections are determined by leading-order perturbation theory from the diagram $q\bar{q} \to Z^0 g$ and $gq \to Z^0 q$. Here the calculation is straightforward.[11] Because of the aforementioned ambiguities in the region $p_T \ll M_Z$ it is however difficult to pinpoint the transition region where leading-order perturbation theory becomes reliable. Guided by the results of Refs. 9, 12, we will here assume that gluon resummation can be neglected for $p_T \geq 20$ GeV so that related problems can be ignored in the present discussion. Our main results are actually confined to the region $p_T \geq 30$ GeV and the experimental puzzle is for $p_T \geq 40$ GeV.

Uncertainties in the leading-order calculation are associated with:

1. Uncertainties in the structure functions. We concentrate here on the parametrizations of Duke and Owens[13] and of Glück, Hoffmann and Reya.[14] The structure functions of Eichten, Hinchliffe, Lane and Quigg[15] do not reproduce the ratio $d_V(x)/u_V(x)$ obtained from electron-scattering data and are not suitable for our study (notice however that the results derived from them are very close to those shown in Figs. 1, 2). The structure functions proposed by Baier, Engels and Petersson[16] are inappropriate for any electroweak process because they assume $u_V(x) = 2\, d_V(x)$, which has been excluded by experimental data. We shall not consider problems related to the fact that structure functions are determined from nuclear-target experiments.
2. Scale of α_s. We let here the strong coupling constant evolve with the scale of the process. Although this scale is clearly defined in the case

$p_T = M_Z$, one is confronted with several choices at lower energies *e.g.* $Q^2 = p_T^2, M_Z^2, \hat{s}$, and in the absence of higher-order calculations it is indeed impossible to decide on a 'best' scale Q^2. Our choices are not even exhaustive as *e.g.* $Q^2 = p_T^2/4$ might deliver the fastest converging series. Also, the different parametrizations of the structure functions lead to different possibilities for the QCD parameter Λ_{QCD} ranging from 0.2 to 0.4 GeV, and thus modify the speed at which α_s evolves.

3. Higher-order effects. The structure functions should be evolved from the energy at which they are measured to the energy scale of the process. This evolution comes from higher-order virtual gluon corrections to $q\bar{q} \to Z^0 g$ and soft-gluon corrections such as $q\bar{q} \to Z^0 gg$. It has been solved and parametrized in the deep-inelastic (DI) case. The Drell-Yan (DY) process can be related to the DI case by crossing the boson and the antiquark lines. The leading-logarithm structure is the same but non-leading corrections can be important at moderate energies. Two corrections arise: one stems from the difference in the final two-body phase-space and will be neglected in what follows. Another comes from the fact that the exchanged boson is time-like in the DY case and space-like in the DI case. One can show[18,17] that the net effect of that sign change is to multiply the cross section by a factor,

$$K = 1 + \frac{\alpha_s}{2\pi}(\frac{4}{3}\pi^2) \qquad (1.1)$$

These corrections are known to be sizeable in interactions dominated by $q\bar{q}$ initiated processes[19] such as $\pi N \to (\mu^+\mu^-)X$ and have been

partially calculated.[20] As these corrections are sizeable, one has to see what the contribution of higher orders would be. We shall adopt here the economical prescription[18]:

$$d\sigma/dp_T^2 = \exp[\frac{\alpha_s(Q^2)}{2\pi}\frac{4}{3}\pi^2] \times [d\sigma/dp_T^2]_{O(\alpha_s)} \qquad (1.2)$$

At our energies, this factor gives a moderate enhancement of 1.3–1.4 to the cross section. The use of the first two terms, as in (1.1), makes only a slight difference.

4. Other uncertainties, such as the experimental resolution of the missing transverse momentum $\not{p}_T \approx \not{E}_T$, will also be briefly discussed.

1.3 RESULTS

Cross Sections The results for the W, Z^0 cross section as a function of transverse momentum, taking into account all the aforementioned ambiguities are shown in Figs. 1, 2. We present them in differential and integral forms; all calculations fall into the bands shown in the figure. The band roughly spans a factor 3 which is the cumulative effect of factors 1.25, 1.6 and 1.35 due respectively to the structure functions, the choice of scale and the K-factor correction. The largest cross sections are obtained for the structure functions of Glück et al.,[14] $Q^2 = p_T^2$ and the inclusion of the K-factor. One might actually favor this choice of scale in $\alpha_s(Q^2)$ and $q(z, Q^2)$ as it directly expresses the fact that the scale of the interaction changes with the transverse momentum of the produced Z^0. As a consistency check, we have computed the production of lepton pairs in $\pi^- N$ interactions. Although comparison

with data[21] is only possible at much smaller values of p_T and $\sqrt{s}$, the confrontation is relevant as it is a $q\bar{q} \to \gamma g$-dominated process in a similar range of $M/\sqrt{s}$ and $p_T/\sqrt{s}$ values. We again investigated a range of pion structure functions. The results shown in Fig. 3 are based on the NA3 π structure functions of Ref. 21; other choices can modify the calculation by up to a factor 1.5. Our assumptions fit the πN data rather well, as can be seen from Fig. 3 and Ref. 19. The analytic result calculated for a nonsinglet combination in Ref. 20 gives a numerically similar factor to our simple parametrization. In summary, we feel that the bands shown in Figs. 1, 2 should be considered as a representative measure of theoretical uncertainties rather than absolute upper and lower bounds. Nevertheless, we shall continue our discussion using the results obtained with the specific set of assumptions yielding the maximal results of Figs. 1, 2.

Implications for $p\bar{p}$ Monojets: Event Characteristics It is clear from Fig. 2 that 1–2 $W \to (e\nu) + jet(s)$ events are expected for $p_T \geq 30$ GeVand 0.7 event for $p_T \geq 40$ GeV per integrated luminosity of 100 nb^{-1}. This is consistent with the rate of $l + \not{p}_T + jet$ events observed in the UA2 data sample[2] and with the observation of one such events by the UA1 group (event A in Ref. 1 and several others in Refs. 1 and 5). Two of the previous UA2 events[2] might still defy explanation. It is however important at this point to remember that experimental resolution can strongly affect this type of comparison as the $\not{p}_T$ distribution is steeply falling. Especially errors on $\not{p}_T$ should be taken into account. They shift the actual p_T value by 5–10 GeV

from the measured one, leading to a significant increase in the expected event rate. A comparison of the calculation with the 1985 sample of $l + \not{p}_T + jet$ data is shown in Fig. 4.a (before background subtraction). In Fig. 5.a we calculated the (W, jet) invariant mass distribution for $p_T \geq 15, 30$ GeV. It is clear that our cross-section predictions are very close to the data. As the ratio of W to Z^0 cross sections is relatively well understood[7,8,10] (see Fig. 6.c), this legitimizes our use of the larger Z^0 cross section to discuss the monojet background.

We have already pointed out that the monojets display the qualitative features expected from the process $Z^0(\to \nu\bar{\nu}) + gluon(s)$: we expect a peak around $p_T \approx 30$ GeV where the detection efficiency for $Z^0 \to \nu\bar{\nu}$ turns on. The corresponding (Z^0, jet) invariant mass is shown in Fig. 5.b for $p_T \geq 15, 30$ GeV covering again the region where the UA1 detector becomes sensitive to the $Z^0 \to \nu\bar{\nu}$ decay. Notice that the Z^0-jet invariant mass is not a measurable quantity in $\not{p}_T$-jet events. However, it can be measured for Z^0 decaying into $l\bar{l}$ or jets. The distribution looks qualitatively like the monojet data[1,5] with a peak expected in the 100–120 GeV invariant mass region. This region is of course further populated by $W(\to \tau\nu) + gluons$ events.

Rates and the Number of Neutrinos As can be seen from Fig. 2, we expect 1–3 Z^0 with $p_T \geq 40$ GeV per 100 nb^{-1}. For three light neutrinos, ($N_\nu = 3$ in Fig. 6), the branching fraction for $Z^0 \to \nu\bar{\nu}$ is 0.2. We therefore expect 'a few' monojets. The question of backgrounds is complex: the UA1 estimate is that 1.5 events above p_T of 40 GeV are due to W decays into leptons.

One has thus 1.5 to 5.5 observed events versus our prediction of 1.5 to 2.8 (assuming that the cuts hardly affect the high-$\not{p}_T$ events of DY origin).

Notice that there is an intrinsic ambiguity in this calculation related to the number of light neutrinos N_ν. For instance, for $N_\nu = 8$, as suggested by some family-unifying theories,[22] the branching ratio $Z^0 \to \nu\bar{\nu}$ is increased by a factor 2 (see Fig. 6). Increasing N_ν augments the total width of the Z^0 and the ratio $R = B\sigma(W \to l\nu)/B\sigma(Z^0 \to l\bar{l})$ as shown in Fig. 6. For $N_\nu = 8$, $\Gamma_Z = 3.7$ GeV is well within present experimental bounds. R is increased to 11.6 ± 0.7 from the standard N_ν value of $R = 8.8$. Notice that the ratio R is predicted with an accuracy far superior to that for individual W, Z^0 cross sections because most uncertainties in the calculation (except that for structure functions) cancel in the ratio.[7,10] This can be used to calculate a bound on the number of light neutrinos, which UA1 reports to be ≤ 7 (see also Ref. 23).

1.4 Conclusion

The present monojet data,[1] although having steered quite a bit of controversy, seem in light of the new UA1 analysis in agreement with the standard model. They can actually be used to set limits on theories predicting monojets, such as mass limits in supersymmetry, or limits on the number of neutrinos.

REFERENCES

1. UA1 Collab., G. Arnison et al., Phys. Lett. **139B**, 115 (1984);
   UA1 Collab., C. Albajar et al., preprints CERN-EP/86-81 (1986) and CERN-EP/86-82 (1986);
   R. Batley, preprint CERN-EP/86-181 (1986).
2. P. Bagnaia et al., Phys. Lett. **139B**, 105 (1984).
3. J.R. Hansen, in Aspen Winter Conference Series, Collider Physics at Ultrahigh Energies (Aspen, CO: January 1985).
4. M. Mohammadi and V. Vuillemin, in Aspen Winter Conference Series (Aspen, CO: January 1985).
5. UA1 Collab., G. Arnison et al., Phys. Lett. **126B**, 398 (1983), Phys. Lett. **147B**, 241 (1984);
   S. Geer, CERN preprint EP/84-160, in Particles and Fields-1984 (Santa Fe, NM: November 1984).
6. F. Halzen and M. Mursula, Phys. Rev. Lett. **51**, 857 (1983);
   D. Cline and J. Rholf, unpublished.
7. K. Hikasa, Phys. Rev. **D29**, 1939 (1984).
8. N.G. Deshpande, G. Eilam, V. Barger and F. Halzen, Phys. Rev. Lett. **54**, 1757 (1985).
9. F. Halzen, A.D. Martin and D.M. Scott, Phys. Lett. **112B**, 160 (1982).
10. G. Altarelli, R.K. Ellis, M. Greco and G. Martinelli, Nucl. Phys. **B246**, 12 (1984).
11. F. Halzen and D.M. Scott, Phys. Lett. **78B**, 318 (1978).

12. P. Aurenche and R. Kinnunen, Phys. Lett. **135B**, 493 (1984);
P. Minkowski, Phys. Lett. **139B**, 431 (1984).

13. D.W. Duke and J.F. Owens, Phys. Rev. **D30**, 49 (1984).

14. M. Glück, E. Hoffmann and E. Reya, Z. Phys. **C13**, 119 (1982).

15. E. Eichten, I. Hinchliffe, K. Lane and C. Quigg, Rev. Mod. Phys. **56**, 579 (1984).

16. R. Baier, J. Engels and B. Petersson, Z. Phys. **C8**, 265 (1978).

17. G. Altarelli, R.K. Ellis and G. Martinelli, Nucl. Phys. **B143**, 511 (1978), Nucl. Phys. **B146**, 544 (1978)(E), Nucl. Phys. **B147**, 461 (1979);
J. Kubar-Andre and F.E. Paige, Phys. Rev. **D19**, 221 (1979);
K. Harada, T.Kaneko and N. Sakai, Nucl. Phys. **B155**, 169 (1979), Nucl. Phys. **B167**, 545 (1980) (E);
J. Abad and B. Humpert, Phys. Lett. **80B**, 286 (1979);
J. Abad, B. Humpert and W.L. van Neerven, Phys. Lett. **83B**, 371 (1979).

18. G. Parisi, Phys. Lett. **90B**, 295 (1980);
G. Curci and M. Greco, Phys. Lett. **92B**, 175 (1980).

19. F. Halzen and D.M. Scott, Phys. Rev. **D24**, 2433 (1978).

20. R.K. Ellis, G. Martinelli and R. Pétronzio, Phys. Lett. **104B**, 45 (1981), Nucl. Phys. **B211**, 106 (1983).

21. NA3 Collab., J. Badier et al., Phys. Lett. **117B**, 372 (1982).

22. J. Bagger and S. Dimopoulos, Nucl. Phys. **B244**, 247 (1984);
J. Bagger, S. Dimopoulos and E. Massó, Nucl. Phys. **B253**, 397 (1985).

23. M. Chaichian and M. Hayashi, Phys. Rev. **D30**, 243 (1984).

FIGURE CAPTIONS

1. Transverse-momentum distribution of W, Z^0 in $p\bar{p}$ interactions with $\sqrt{s}$ = 630 GeV. The W scale has been shifted upwards by a factor 10. The theoretical errors (not necessarily upper/lower limits) are described in the text.
2. Integral distributions corresponding to the transverse-momentum distribution shown in Fig. 1. The scale on the right-hand side gives the number of W, Z^0 events passing a minimum p_T cut p_T^0 for an integrated luminosity of 100 nb^{-1}. Predictions for $\sqrt{s}$=540 and 630 GeV are shown separately.
3. A calculation of the transverse-momentum distribution of lepton pairs in πN interactions, based on identical assumptions to those resulting in the largest W, Z^0 cross sections shown in Figs. 1, 2, is compared to the data of Ref. 21. The discrepancy with the low energy data can be accounted for by the intrinsic transverse momentum of the colliding partons.[19,20]
4. Comparison of $l - \not{p}_T - jets$ and $\not{p}_T - jet(s)$ data of Refs. 1-4 with the standard-model predictions for $\sqrt{s}$ =630 GeV. The event rate was obtained by normalizing each event to the luminosity of the sample in which it has been observed. No corrections for detection efficiency have been applied. We assumed a branching ratio B($W \to l\nu$)=1/12 in (a) and B($Z^0 \to \nu\bar{\nu}$)=0.2, 0.4 in (b). This corresponds to the standard model with three (solid line) and eight (dashed line) light neutrinos. Also shown in (b) is the Z^0 transverse-momentum distribution shifted by 8 GeV in order to illustrate the importance of errors in the $\not{p}_T$ measurements. A gaussian experimental resolution of 10 GeV for $\not{p}_T$ would increase the apparent cross section, shifting the scale by $\approx$ 5 GeV.
5. Invariant mass of the W-jet and the Z^0-jet system corresponding to the larger transverse-momentum distribution shown in Fig. 1. Separately shown are the results for a minimum transverse momentum of the jet (or W , Z^0) equal to 15, 30 GeV.
6. Standard-model predictions for the total width, the branching ratio into neutrinos of the Z^0 bosons and the ratio of the number of W^{+}_{-} to Z^0 events observed in a definite $l\nu, l\bar{l}$ leptonic mode as a function of the number of light neutrinos. Errors in (c) have been obtained using the same procedure leading to the errors in Fig. 1. The error for the ratio is much smaller than that for the individual cross sections.

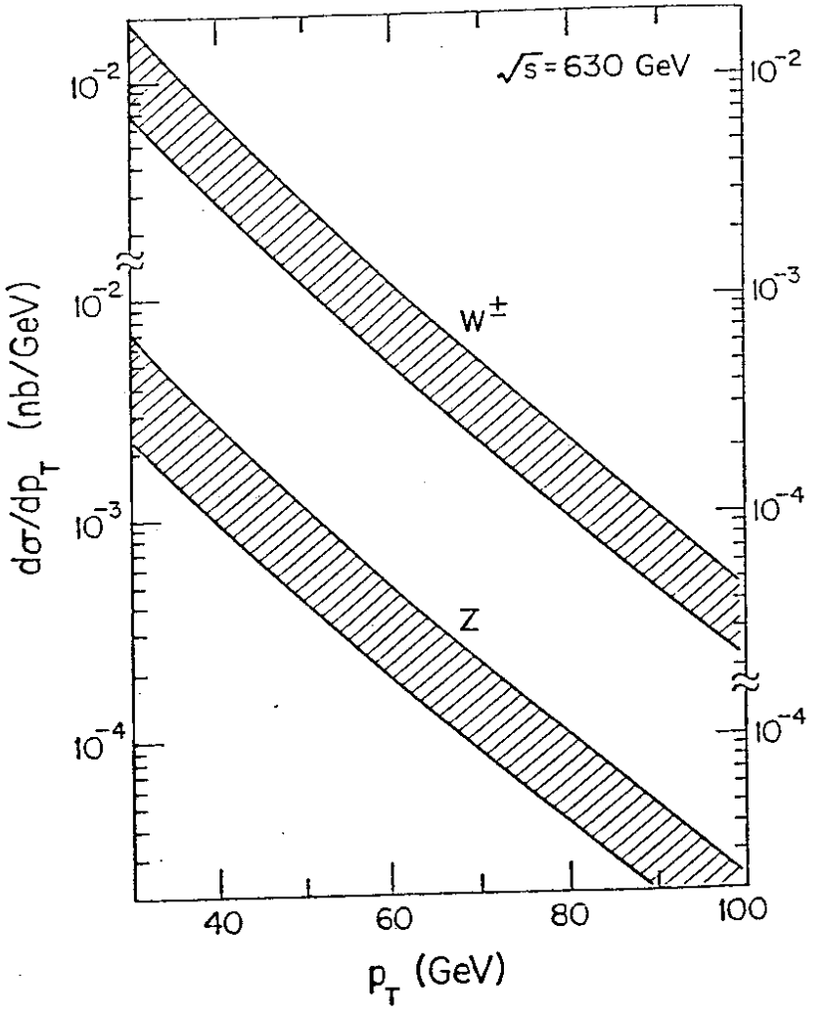

Figure 1

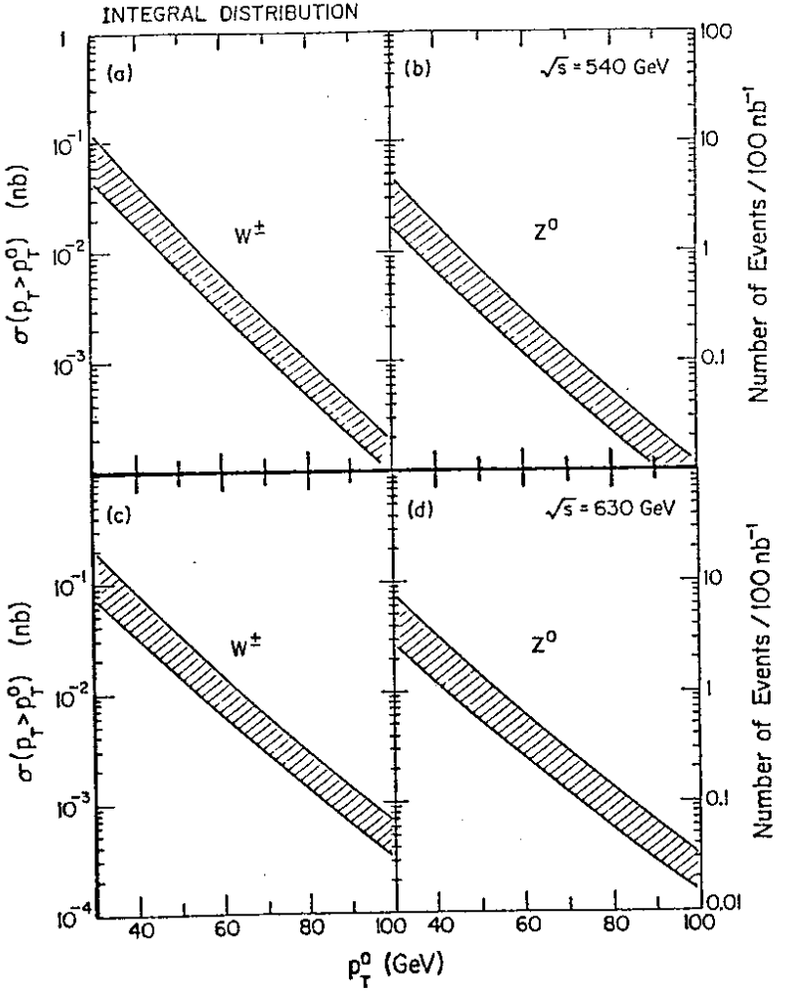

Figure 2

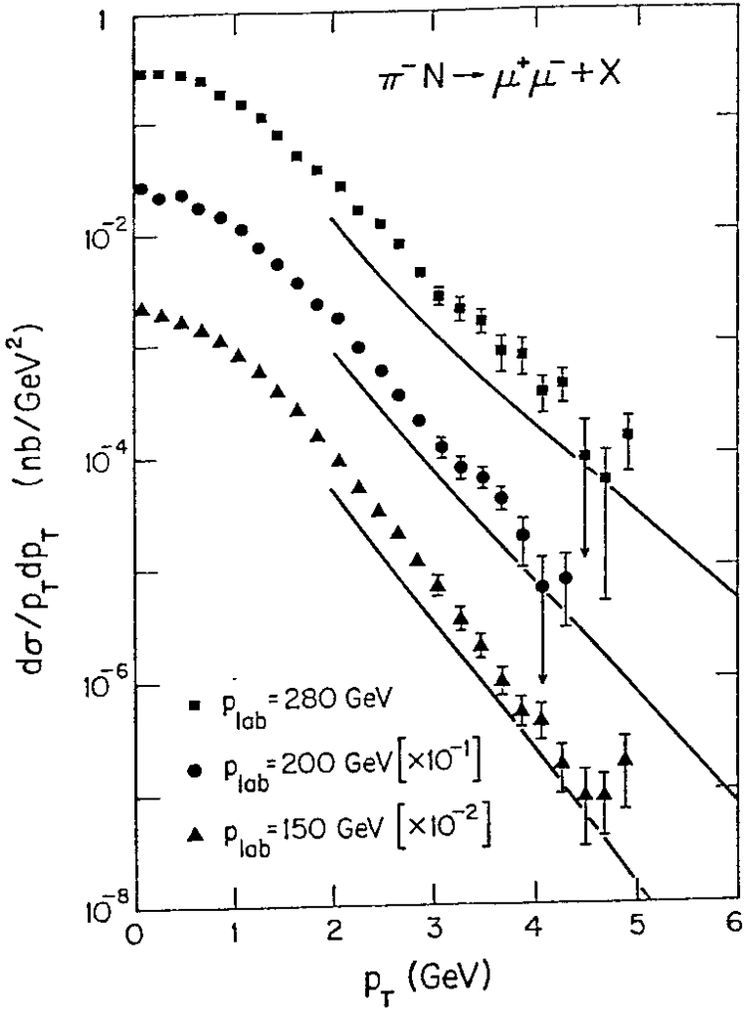

Figure 3

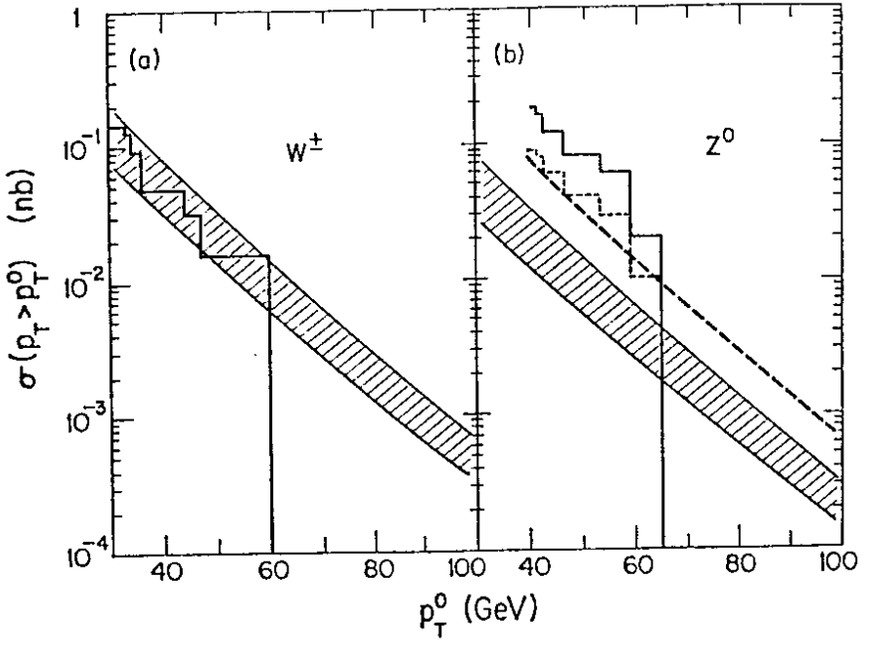

Figure 4

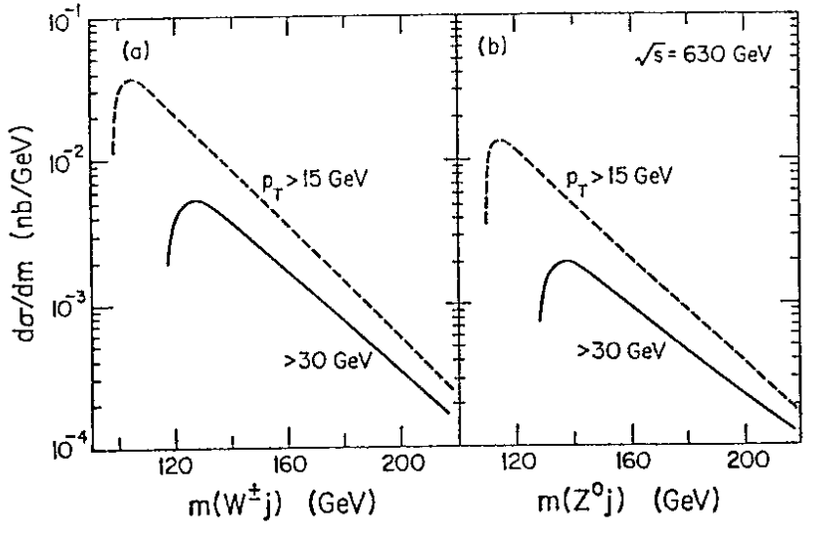

Figure 5

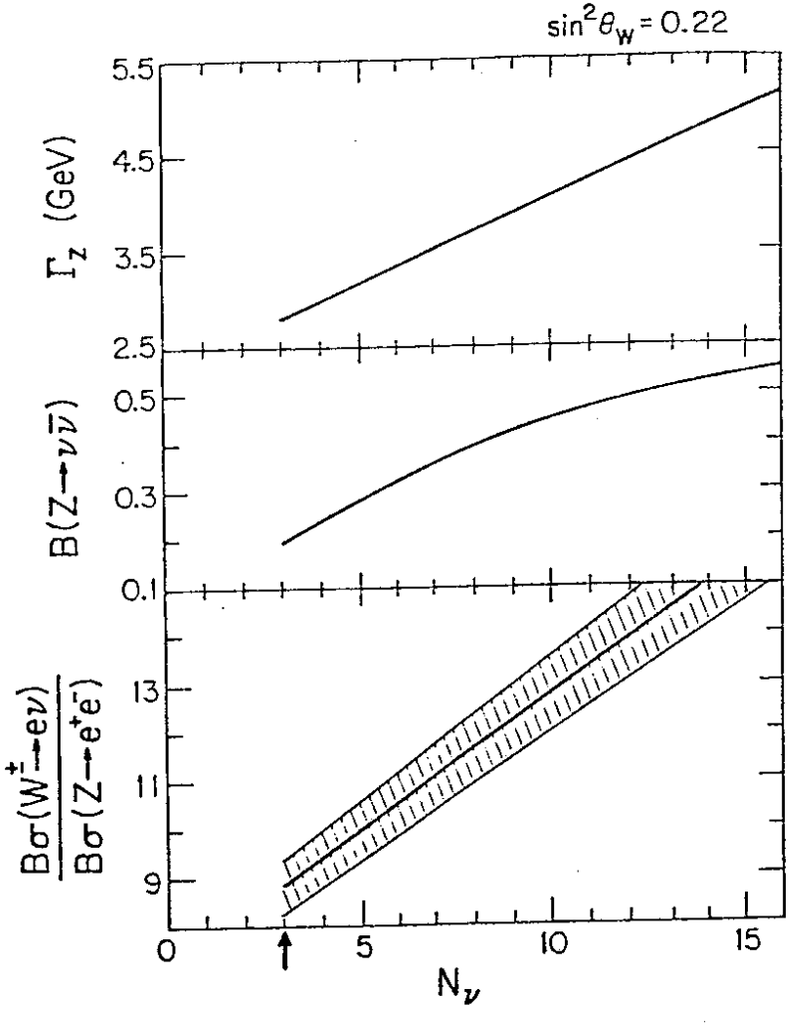

Figure 6

CHAPTER 2

Charm Hadroproduction

2.1 Introduction and Discussion of the Data

In this chapter, we reconsider the problem of charm hadroproduction[1] Several beam-dump experiments[2] have reported cross sections exceeding the standard-model estimates by several orders of magnitude. Before embarking in a theoretical re-analysis of the problem, we need to examine what are the experimental problems related to these measurements?[2–4]

Most experiments are performed using heavy nuclear targets, so that the A-dependence is a necessary tool for deriving the single-nucleon cross section.

- ◇ This dependence can be parametrized in the total cross section case as $\sigma(A) = A^{\alpha}\sigma(p)$. α has been measured in proton-induced reactions and appears to be strongly dependent on Feynman x_F, and ranges from 0.75 to 0.45. It is unclear if this effect is beam or energy dependent.
- ◇ For charm production however, α has been measured to be 1 on Pt (NA3) and 0.77 on Be, Cu and W (E613 and BIS-2).

Several other factors can lead to sizeable corrections in the measured result, such as the range of x_F considered, the cuts in the data (from trigger inefficiencies, dead zones in the apparatus, limited angular acceptance...).

We thus draw attention to a recent measurement by the LEBC bubble chamber that the D cross section in pp interaction is $22\,\mu$b with a small error?[2,5] This experiment has large acceptance and is done on a hydrogen

target. No large phase-space corrections are involved in obtaining the result, the error is essentially statistical. We speculate that the discrepancy between the perturbative calculation and the data might be illusory and associated with large ambiguities in the calculation, which we shall now review.

2.2 Perturbative Charm Hadroproduction

Validity of the Perturbative Approach: Fusion and Other Mechanisms

Perturbative QCD is defined only for short-distance processes. In other words, this says that quarks can be on mass-shell for a very short time and to ensure this, one needs the quark to interact with another particle which is very much off mass-shell. This 'off-shellness', *i.e.* the difference between the squared four-momentum of the particle and its squared mass, defines the energy scale of the process. It enters the expression of the running coupling constant α_s and makes it small, so that the quarks behave as almost-free particles and the perturbative sum can be truncated. Hence, a perturbative QCD calculation makes sense only if there is a big off-shellness in the problem and the tree approximation is valid only if α_s is small at this scale.

The leading-order diagram for production of charm, or of any other heavy quark is the gluon-fusion process (see Fig. 1.a). In this case, the exchanged quark is in the t channel and its squared four-momentum is negative. It is thus off-shell by an amount at least equal to its mass squared m^2, and the lifetime of the intermediate state is of order $1/m$. Perturbative QCD applies here. The size of α_s is controlled by the ratio $m/\Lambda_{\rm QCD}$. In the case of charm, $0.27 \leq \alpha_s(m_c^2) \leq 0.44$ for 0.1 GeV $\leq \Lambda_{\rm QCD} \leq$ 0.2 GeV and

1.1 GeV $\leq m_c \leq$ 1.5 GeV. The next-to-leading order should thus contribute by a factor $\approx \alpha_s/\pi \leq 15\%$.

This leading diagram naïvely gives an answer ≈ 10 lower than the measured values, at least for $m_c = 1.5$ GeV. Several authors have considered other sources for charm, and we shall here follow Ref. 6 to argue that these alternatives are not legitimate uses of perturbative QCD.

We shall first consider the main alternative to gluon fusion: 'flavor excitation' (see Fig. 1.c), *i.e.* the process through which a sea charm quark is excited out of the proton. First of all, this graph is infrared divergent due to the collinear singularity accompanying the massless gluon. The contribution of the infrared cut-off Q_0 behaves like $1/Q_0^2$, greatly limiting the predictive power of such a contribution. Moreover, only part of these graphs should be included in the perturbative calculation and one should identify carefully the hard-scattering process. One can indeed rewrite them as in Fig. 1.d, which shows that the virtuality of the exchanged quark is bigger than that of the intermediate gluon. The quark thus cannot be put on shell, and the hard scattering is partially hidden in the structure function. Also, rewritten as Fig. 1.d, the graph is clearly a higher-order contribution to the fusion diagram and is suppressed by an extra factor α_s/m_c^2. Written this way, this is essentially what one calls diffractive production of charm. The observation of charm particles with large longitudinal momentum, first believed to be the signature of diffractive production, is now believed to be the consequence of a boost in momentum of the charm quark (produced with low x by the fusion mechanism) resulting from the pick-up of spectator valence quarks to form a charm particle D, A_c (for further discussion on diffractive production of heavy quarks, see Ref. 7 on the theoretical side and Ref. 8 on the experimental side).

Other production mechanisms have been proposed, such as 'prebinding distortion'. For a discussion of these alternatives, see Ref. 6 where it is argued that only fusion processes are within the realm of perturbation theory.

To summarize, higher-order contributions might provide a big contribution to the cross section (similar to the K-factor in Drell-Yan, see Chapter 1), but a complete calculation of these higher-order graphs (which is not available yet) would be needed to be consistent with perturbation theory. Non-perturbative effects are typically suppressed by a factor $1/m_c^2$ and could also be important in the case of charm. We shall however limit ourselves to the tree-order cross section and reevaluate how far it is from the experimental results.

Importance of the Mass in Hadroproduction As discussed above, heavy quarks are produced, to leading-order, via the fusion diagrams $q\bar{q} \to c\bar{c}$ and $gg \to c\bar{c}$. The heavy quark threshold is implemented in the calculation by requiring that $s_{q\bar{q}}, s_{gg} \geq 4m_c^2$ in diagrams such as those of Figs. 1.a-b. Here m_c is a threshold parameter which is related, but not necessarily identical, to the quark mass obtained from considering nonrelativistic charmonium model. It is well-known[9] that the cross section for charm production is very sensitive to the value of m_c. This is illustrated in Fig. 2.a for $\sqrt{s} = 27.4$ GeV and for

various choices of structure functions![10] The origin of the strong dependence of the predicted cross section on m_c is the very rapid dependence of the structure functions on s_{gg} (or $s_{q\bar{q}}$) which are integrated above the threshold $x = 2\,m_c/\sqrt{s_{gg}}$. We shall thus carefully reconsider how one defines the quark masses.

The Definition of Quark Masses Quarks have not been observed as free particles. This means that their inertial properties are not straightforwardly defined. On the other hand, QCD is a renormalizable theory, which means that all infinities of loop calculations can be absorbed in the redefinition of a finite set of constants. Typically, as in QED, one would want to use to this effect the masses and charges which enter the bare Lagrangian. However, due to confinement, these masses are not available, so that one has to use other observable quantities to define the theory. The problem is then to relate these to the constituent masses.

Indeed, before using this approach, one has to define the quark masses in some way within perturbation theory. The quark propagator is rewritten:

$$S(p) = Z(p^2)[M(p^2) - \not{p}]^{-1} \tag{2.1}$$

and one has to determine the value of the quantity $M(p^2)$ at the space-like point $p^2 = -4\ m^2_{quark}$ to define the theory. The functions $M(p^2)$ and $Z(p^2)$ can be expressed in terms of the running mass $m(Q^2)$ and the running coupling constant $\alpha_s(Q^2)$ order by order. These are gauge-invariant quantities, and the equation $m(4\ m^2) = m$ unambiguously defines a quark mass m

to all orders of perturbation theory. In the Landau gauge, using the $\overline{\rm MS}$ subtraction scheme and to one-loop order, the relation between M and m is:

$$M(-4\ m^2) = m(4\ m^2)[1 + \frac{\alpha_s}{\pi}(4/3 - 2\ \ln 2)] \approx m(4\ m^2) \tag{2.2}$$

In the following, we shall use the following parametrization of the running mass:

$$m_c(q^2) = m_0 \times \left(\frac{\log(4\ m_0^2/\Lambda^2_{\rm QCD})}{\log(q^2/\Lambda^2_{\rm QCD})}\right)^{\frac{12}{25}} \tag{2.3}$$

One is thus confronted with the determination of $m_0 \equiv m_c(4\ m_c^2)$. Three types of experimental results can define this quantity.

- ◇ First, one can use QCD sum rules[11] for the vacuum polarization amplitude to derive the heavy quark masses from e^+e^- data. The best value, to the one-loop order, is given by:
  $m_0 = (1.27 \pm 0.05)$ GeV.
- ◇ Secondly, one can use nonrelativistic-potential-model estimates. Their best fit to the charm quark mass is $m_c = 1.65$ GeV. However, the connection between this estimate and the current mass m_0 is not clear. Notice first that the mass M (and so m) is defined in (2.2) for negative momentum transfers: the propagator of a quark looks like a free fermion propagator only as long as p^2 stays away from $[m(4\ m^2)]^2$, where non-perturbative methods would have to be used to get a reliable representation of the propagator. Within perturbation theory, the physical mass of a quark seems however to be a well-defined concept

and this is used to relate the current mass to the potential-model mass. The Balmer formula, which one uses to extract this estimate has to be corrected for non-perturbative effects. These have been worked out in the case of the b quark, but in the case of charm, one expects the result to break down and the definition of a quark physical mass to be of little use. The estimate one gets through this approach is:
$m_0 \approx 1.4$ GeV.

◇ One can finally use a perturbative approach, where one treats the charm quark as a small parameter breaking the $SU(4) \otimes SU(4)$ chiral current symmetry of the massless theory. As the mass of the charm quark is of the same order as the QCD scale, one does not expect the outcome to be very accurate. From the mass formulae for the pseudoscalar and the vector multiplets, one gets the estimate:
$m_0 \approx 1.25$ GeV.

As a conclusion, we see that considerable ambiguities are involved in the determination of the charm quark mass. Most of the estimates hint at a value between 1.22 and 1.4 GeV. The charm-hadroproduction cross section, dominated by the space-like exchange of a charm quark, should thus be considered as a measurement of the parameter m_c rather than a check of perturbative QCD.

2.3 Results

In order to reconcile the LEBC result with leading-order QCD we require that $m_c \lesssim 1.25$ GeV. The value could be smaller because Λ_c, F, ... productions are not included, see Fig. 2. We have considered fixed quark masses so that one may compare with the previous calculations. Allowing the quark mass to run according to Eq. 3 does not significantly modify the result. Notice that the mass range we get is perfectly consistent with the present estimates of current masses.

A critical test of the suggestion that the normalization of the gluon-fusion diagrams be increased by choosing $m_c < \frac{1}{2} m_\psi$ is that all other predictions of the model, which are not noticeably affected by the shift in mass, be correct. In other words, the Feynman x_F and transverse-momentum dependence of the cross section as well as the correlation between the charm particles produced have to be consistent with the predictions of the leading-order fusion calculation (see Fig. 3). Recent experiments show that this is indeed the case.[2]

Tests of this Approach

This resolution of the charm-hadroproduction puzzle can be tested in two obvious ways. One is the cross section in πp interactions. The results are shown in Fig. 2.b. Our calculation with smaller m_c again agrees with the data,[12] although the gluon distribution in pion is not known well (we used the Q^2-dependent parametrizations of Owens[13]).

The second test directly involves measurement of the energy dependence of the charm cross section. In Fig. 4 we calculate the ratio of the pp cross section at 800 and 400 GeV. For the low values of the threshold-parameter m_c the energy dependence of charm production is less strong than for previous calculations using $\frac{1}{2}m_\psi$ or m_D. A measurement of this ratio has been published recently, using Fermilab's doubler. We predicted an increase in the cross section of less than a factor $\lesssim 1.8$ from 400 GeV to 800 GeV where previously an increase of a factor 2.5 or more might have been expected. Fig. 4 compares our prediction with the data[14] and Fig. 5 gives our prediction for $\sqrt{s}$ in the interval 10–120 GeV. We see that fusion diagrams give a correct answer only for the structure functions[10] of Duke and Owens (set 2) and of Glück et al.. The parametrization of Eichten et al. gives a wrong estimate, which is to be expected as these structure functions work very poorly at low energies and for hadronic processes.

2.4 Conclusion

Both high-energy $p\bar{p}$ collider and fixed target experiments seem to be consistent[8] with leading-order QCD, although there might be some corrections. The evidence for unconventional sources of heavy quarks now rests mainly on ISR experiments. Given their complicated triggers and their small phase-space coverage they might have been misinterpreted as to the precise values of the cross section and the momentum distribution of the quarks.

REFERENCES

1. J.R. Cudell, F. Halzen and K. Hikasa, Phys. Lett. **B157**, 447 (1985).
2. C. Caso, in *Proceedings of the 1985 International Symposium on Lepton and Photon Interactions at High Energies*, Kyoto, edited by M. Konuma and K. Takahashi (Kyoto: Kyoto University, 1986), p. 488.
3. M.E. Duffy *et al.*, Phys. Rev. Lett. **55**, 1816 (1985).
4. M.E. Duffy *et al.*, 'Characteristics of charm production by 400 GeV protons,' University of Wisconsin preprint WISC-EX-86-262 (1986).
5. A. Goshaw *et al.*, talk given at the Oregon DPF Meeting, Eugene, Oregon, Aug. 12–15, 1985, unpublished.
6. J.C. Collins, D.E. Soper and G. Sterman, in *Proceedings of th Oregon Workshop on Super High-Energy Physics*,Eugene, Oregon, 1985, p. 292
7. R.K. Ellis, 'Forward production of heavy flavors in proton nucleus scattering,' preprint Fermilab-Pub-86/35-T (1986).
8. F. Halzen, in *Proceedings of the Oregon Meeting*, Eugene, Oregon, 1985, edited by R.C. Hwa (Singapore: World Scientific, 1986), p. 529.
9. For a recent discussion, see:
   B.L. Combridge, in *New Flavors, Proceedings of the Second Moriond Workshop*, Les Arcs, 1982, edited by J. Tran Thanh Van and L. Montanet (Gif-sur-Yvette: Edition Frontières, 1982), p. 451;
   F. Halzen, same proceedings, p. 471;
   R.J.N. Phillips, same proceedings, pp. 463 and 467.

10. J.F. Owens and E. Reya, Phys. Rev. **D17**, 3003 (1978);
M. Glück, E. Hoffmann and E. Reya, Z. Phys. C **13**, 119 (1982);
D.W. Duke and J.F. Owens, Phys. Rev. **D30**, 49 (1984);
E. Eichten, I. Hinchliffe, K. Lane and C. Quigg, Rev. Mod. Phys. **56**, 579 (1984).

11. V.A. Novikov *et al.*, Phys. Rev. Lett. **38**, 626 (1977); Phys. Lett. **67B**, 409 (1977); Physics Reports **41**, 3 (1978);
L.J. Reinders, H.R. Rubinstein, and S. Yazaki, Nucl. Phys. **B186**, 109 (1981);
J. Gasser and H. Leutwyler, Physics Reports **87**, 77 (1982).

12. LEBC-EHS Collaboration, M. Aguilar-Benitez *et al.*, 'Charm hadron properties in 360 GeV/c $\pi^- p$-interactions,' preprint CERN/EP/85-103, submitted to Z. Phys. C.

13. J.F. Owens, Phys. Rev. **D30**, 943 (1984).

14. LEBC-MPS Collaboration, R. Ammar *et al.*, Phys. Lett. **B183**, 110 (1987).

FIGURE CAPTIONS

1.a Gluon-fusion diagram. h_1 and h_2 are incoming hadrons (pions or nuclei), g are gluons lines, q light quarks and c the charm quarks.

1.b Quark fusion diagram.

1.c Charm excitation diagram.

1.d Diffractive production of charm.

2.a Cross section for charm production in proton-proton interactions with $\sqrt{s} = 27.4$ GeV as a function of the threshold- parameter m_c appearing in the calculation of the leading-order $q\bar{q} \to c\bar{c}$, $gg \to c\bar{c}$ diagrams. The band represents different choices of structure functions.[10] We use a running coupling constant with $\Lambda_{\rm QCD}$ appropriate for the corresponding structure function. The running scales are fixed at $4m_c^2$. The data[5] on D production are shown as a lower limit on the charm cross section.

2.b Same as 2.a for πN interactions.

3. Charm x_F distribution at ISR calculated with the structure functions of Glück *et al.*[10] and a charm mass 1.2 GeV $\leq m_c \leq$ 1.3 GeV.

4. Ratio of charm production cross sections at 800 GeV and 400 GeV for the calculations shown in 2.a and compared with the present data.[14] The plain horizontal line represents the LEBC upper bound for the ratio and the dotted horizontal line gives their best value.

5. Charm-hadroproduction cross section as a function of $\sqrt{s}$ for the parametrization of Fig. 3.

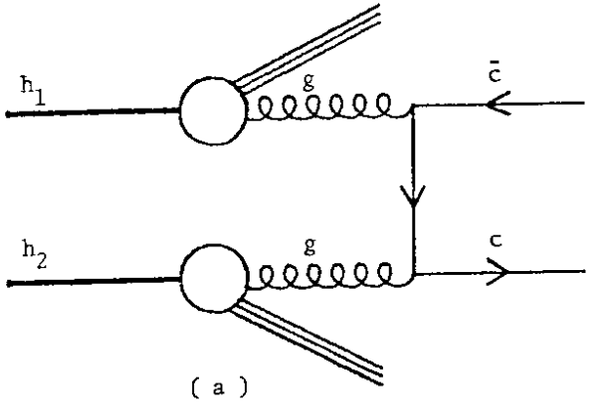

(a)

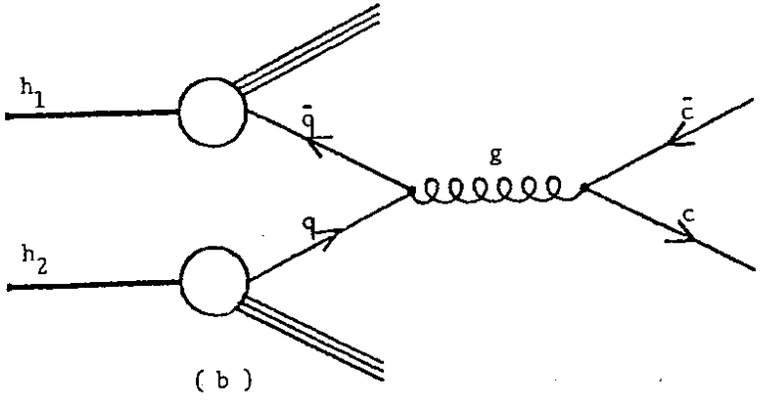

(b)

Figures 1.a and 1.b

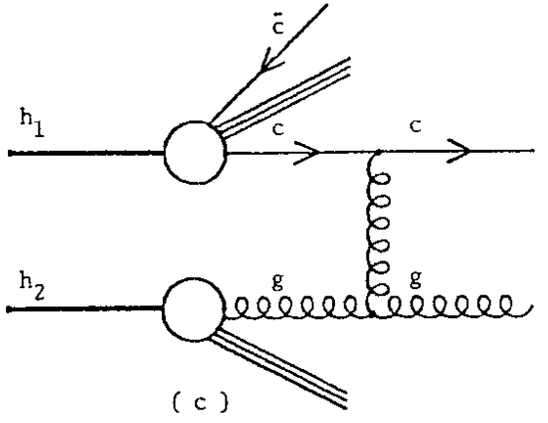

(c)

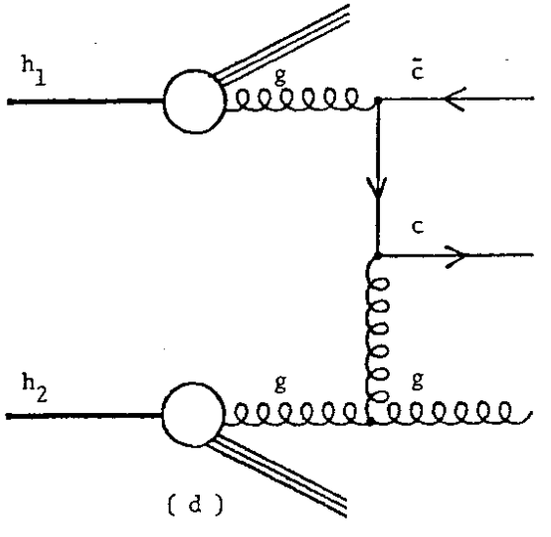

(d)

Figures 1.c and 1.d

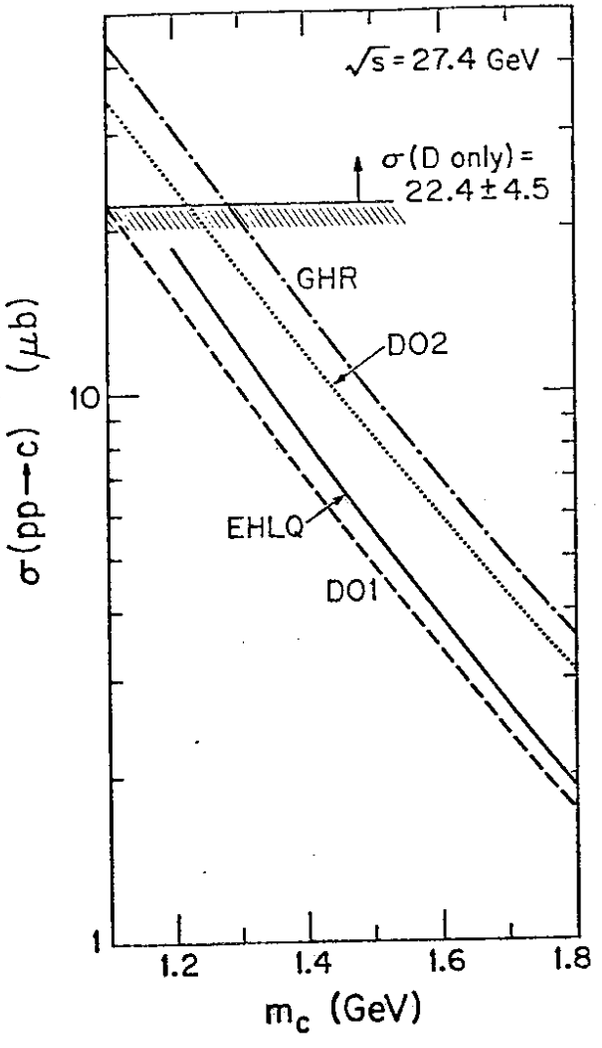

Figure 2.a

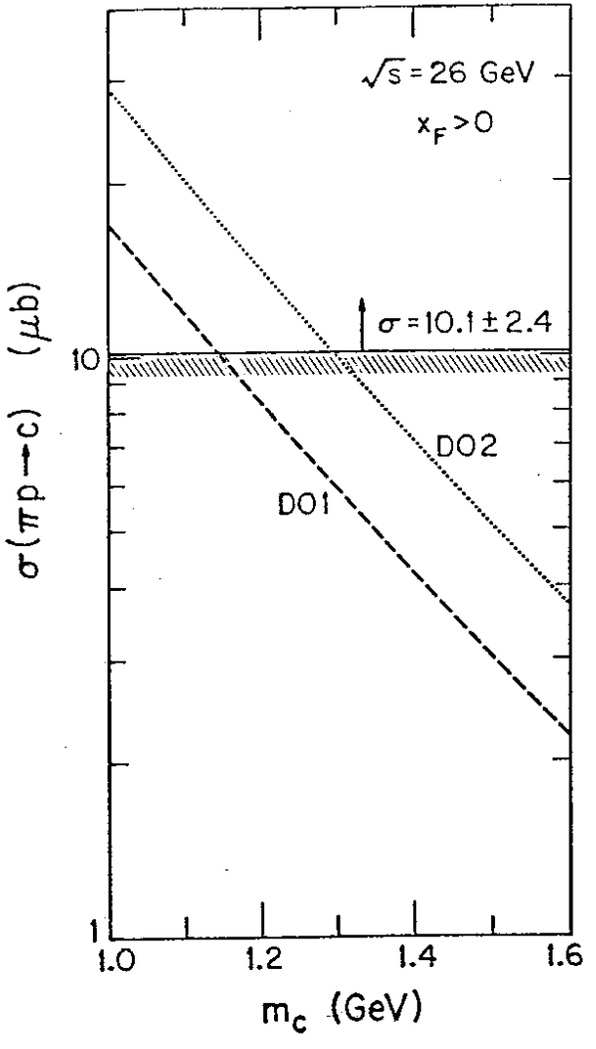

Figure 2.b

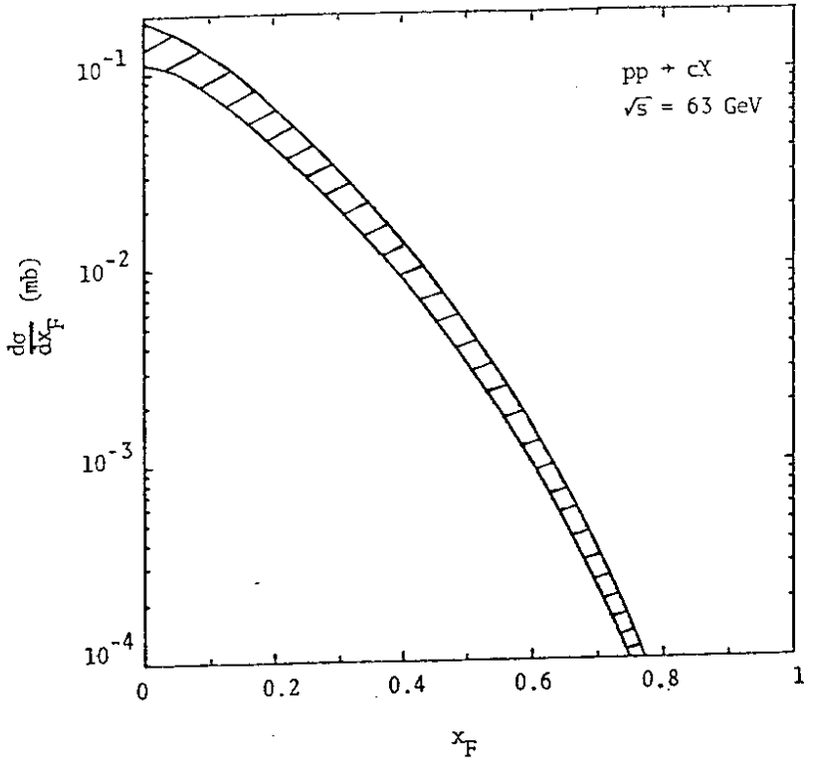

Figure 3

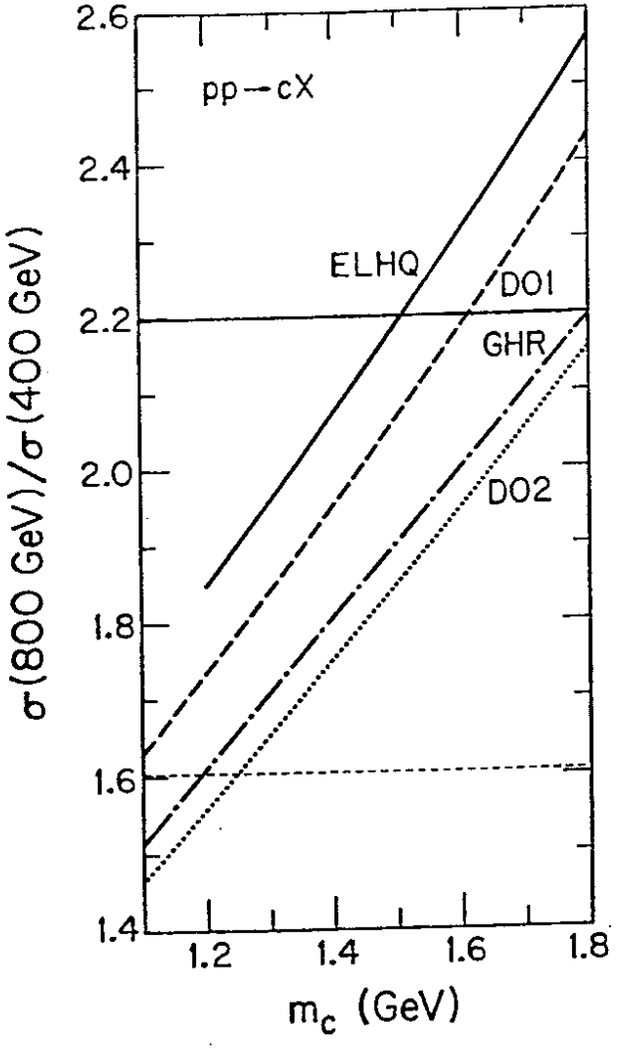

Figure 4

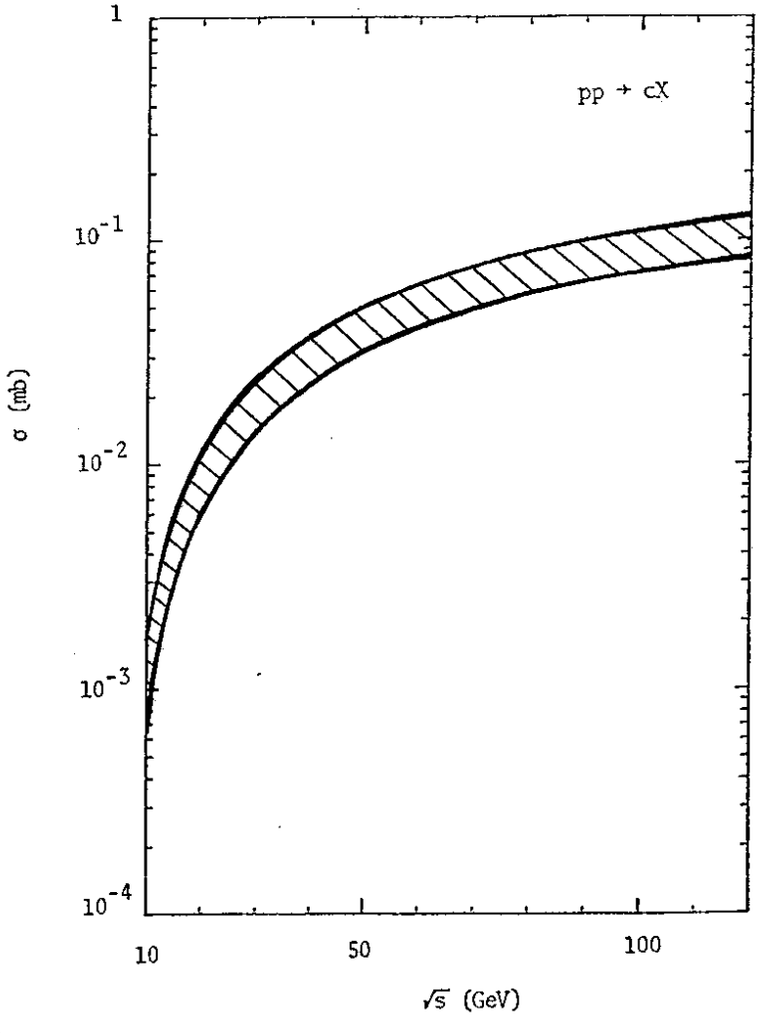

Figure 5

CHAPTER 3

The Same-Sign-Dilepton Puzzle

3.1 Motivation and Discussion of the Data

Except for occasional warnings[1] we have routinely ignored the fact that the standard model fails to accomodate the experimental data[2,3] on the production of same-sign dimuons in the interaction of neutrinos with hadrons. We reconsider[4] this problem in view of the confirmation of the earlier results by an experiment[5] with five times the sensitivity of earlier measurements.

These data were obtained with the CDHS detector exposed to three different neutrino beams, a 300 GeV narrow-band beam (NBB) with very low antineutrino background but low intensity, two 400 GeV wide-band beams (WBB), one mainly neutrino and the other mainly antineutrino. The neutrino and antineutrino spectra are measured from the charged-current process $\nu(\bar{\nu})\ nucleon \rightarrow \mu^-(\mu^+) + X$ which has a cross section σ_{cc} proportional to the neutrino energy. The theoretical calculation will have to be averaged over these spectra (see Fig. 1). The detector used had a large geometrical muon acceptance (≈ 1), a large fiducial mass (therefore increasing the event rate) and a small hadron mean-free path (thus limiting the data to prompt events).

For each event, the muon energies $E_\mu^{(1)}$ and $E_\mu^{(2)}$ and the hadron-shower energy E_H were measured. The data were divided into three bins of visible energy $E_{vis} = E_\mu^{(1)} + E_\mu^{(2)} + E_H$: 3–100 GeV, 100–200 GeV and 200–300 GeV. In general, E_{vis} is different from the neutrino energy as one neutrino

is usually missing. In the case of opposite-sign dimuons, the average missing energy is $\approx 12\%$. We shall assume in the following that a shift of 12% in the neutrino energy is a good representation of this effect. Notice on the one hand that in the same-sign-dimuon case the neutrino is on the average softer than in the opposite-sign case. The number one gets from a Monte-Carlo study[6] based on our calculation is $\approx 7\%$. On the other hand, the uncertainty on the energy in the calculation of the incoming neutrino spectra comes from the muon-momentum determination $\frac{\Delta p}{p} \approx 9\%$ and from the hadronic energy[2] $\frac{\Delta E_h}{E_h} \approx \sqrt{\frac{1\ \mathrm{GeV}}{E_h}}$. This smearing has not been corrected for in the CDHS fluxes and due to the rapidly falling spectra, its net effect is to shift the neutrino energy $\approx 5\%$ higher, or the visible energy $\approx 5\%$ lower. The two effects thus compensate to roughly reproduce the original 12%.

Finally, the produced muons are divided into three bins, with cuts on both muon momenta of respectively 6 GeV, 9 GeV and 15 GeV. These cuts have to be smeared due to the uncertainty in the muon momentum.

The backgrounds to this process come mainly from π and K decays. These have been carefully discussed in Ref. 2. We simply want to emphasize here the fact that the background subtraction is very severe at low energy (signal/background $\approx 25\ \%$) and is reduced by the cut on muon momentum.

3.2 Perturbative vs. Non-Perturbative Contributions

The leading diagrams for the production of same-sign dimuons in the standard model are shown in Fig. 2. The second muon is of charm pair origin, *i.e.* $O(\alpha_s^2)$ in QCD, as the leading $O(1)$ diagrams such as $\nu s \to \mu^- c(\to \mu^+)$

only result in opposite-sign leptons. It is a long-standing puzzle[1] that a routine calculation of the diagrams in Fig. 2 falls short of the measurements by 1 to 2 orders of magnitude.

As the experimental signal is now well established one might be inclined to question the theoretical interpretation and blame the signal on soft, non-perturbative effects. This road has been traveled[7] and such an apology for the discrepancy between theory and experiment can actually be dismissed! We briefly review the arguments.

Large same-sign-dimuon cross sections are supposed to be associated with a large non-perturbative probability for a quark jet, produced in a charged-current interaction, to fragment into a $c\bar{c}$ pair, see Fig. 3.a. The fragmentation function $D_{u\to c\bar{c}}$ can be adjusted[7] to describe the data. But as a result, a large non-perturbative charm production component is now predicted by factorization in hadron collisions, see Fig. 3.b. This component would be diffractive in nature and a recent Fermilab beam-dump experiment[8] limits the cross section of such a charm source to $30\,\mu$b if it is present in the data at all. Therefore,

$$D_{u\to c\bar{c}} \simeq \frac{\sigma_c}{\sigma_\pi} = \frac{n_c^{-1}\sigma(NN \to cX)}{n_\pi^{-1}\,\sigma(NN \to \pi X)} \lesssim 10^{-3} \qquad (3.1)$$

This puts a bound on the dimuon signal by factorization of the diagrams in Fig. 3:

$$\frac{\sigma(\mu^-\mu^-)}{\sigma(\mu^-)} \simeq B(c \to \mu)\ D_{u\to c\bar{c}} \lesssim 10^{-4} \qquad (3.2)$$

Hadron data at $\sqrt{s} \simeq 30$ GeV put a bound on dimuons from a neutrino beam with $E_\nu > 150$ GeV and therefore Eq. (3.2) falls short of the data. Notice that neutrino and hadron interactions in Fig. 3 should be compared at the same center-of-momentum energy of the u-quark, *i.e.*

$$s_{NN} = \langle x \rangle^{-1} \, s_{pN} = \langle x \rangle^{-1} \, s_{WN} \tag{3.3}$$

with $s_{WN} = 2M\nu - Q^2$. Here $\langle x \rangle \simeq 0.2$ corrects[9] for the leading-particle effect. For $Q^2 \simeq 70$ GeV^2 we indeed see that $E_\nu \simeq 150$ GeV corresponds to $\sqrt{s_{NN}} \simeq 30$ GeV. We also used $n_c = 1$ rather than 2 in Eq. (3.1) as only the forward (large x) charm particle is subject to the 30 μb limit.

Moreover, any explanation of the same-sign-dimuon puzzle along these lines implies the existence of truly diffractive charm production in hadron collisions with an observable cross section in the Fermilab/SPS energy range. Data do not seem to support this. On the theoretical side, the existence of such a large soft (intrinsic) charm component of the proton has been shown[10] to be inconsistent with QCD. The arguments developed in Chapter 2 for charm hadroproduction can indeed be directly transposed to this case.

Same-sign dimuons can also result from D^0–$\bar{D}^0$ mixing and b-quark production followed by the cascade decay $b \to c \to \mu$. The cross sections are, however, very small![11]

We therefore question whether the same-sign-dimuon puzzle can be dismissed as a soft physics problem.

3.3 Discussion of the Perturbative Calculation

The matrix element corresponding to the diagrams of Fig. 2 is well-known, and we shall refer the reader to Ref. 11 for the explicit expression (notice a misprint: one should have $g \cdot g - 2\ d \cdot g$ instead of $g \cdot g + 2\ d \cdot g$ in the propagator factor of formula 6), and to Appendix A for the details of the kinematics.

As in the case of charm hadroproduction (see Chapter 2), we speculate that the discrepancy between the perturbative calculation and the data might be illusory. In the present case, the theoretical ambiguities are again mainly associated with the treatment of the $c\bar{c}$ threshold. We shall now consider them in detail.

The Charm-Quark Mass As discussed in Chapter 2, the charm mass that should enter the calculation is the current mass $m_c \approx 1.25$ GeV. We shall consider a running mass given by Eq. (2.3). The dependence on the quark mass is even more severe than in the fusion case of Chapter 2, as the effect of the the gluon propagator gets reinforced by the light-quark propagator.

The Charm Fragmentation The production of muons mainly comes from the fragmentation of charm into D mesons, followed by the decay $D \to \nu\mu + X$. The muons follow the D direction, so that we can represent the decay in the collinear approximation by a fragmentation function

$$D_{D\to\mu}(z) = 2\ (1-z)^2(1+2z) \tag{3.4}$$

with z the fraction of the D momentum carried away by the muon. We thus have to fold in the usual way this decay distribution with the quark fragmentation function:

$$D_{c\to\mu} = \int_z^1 \frac{dy}{y} D_{c\to D}(\frac{z}{y}) D_{D\to\mu}(z) \tag{3.5}$$

We are then left with the determination of the $c \to D$ fragmentation function![12] The most reliable experimental results come from e^+e^- annihilation. It is found there that the Peterson fragmentation functions, based on independent fragmentation, do not reproduce the observed D transverse-momentum spectrum. The Lund Monte-Carlo gives a much more realistic result but is not implementable in a simple calculation. One can however use a phenomenological ansatz which reproduces well the central part of the x_F production region:

$$D_{c\to D} = \delta(z - \bar{z}) \tag{3.6}$$

The e^+e^- data are best described by $\bar{z} = 0.68$, but for the present calculation, we used the value $\bar{z} = 1$ which is known to adequately describe[13] hadronization of charm quarks in a description of hadroproduction in terms of gluon fusion. The fact that this is not the fragmentation function measured in $e^+e^- \to c\bar{c}$ is not directly relevant because of the quite different environment.

The Scales of the Problem Two scales Q_W and Q_g are involved in this process and correspond respectively to the weak-boson and to the gluon momentum transfers. Q_W controls the evolution of the structure functions,

and Q_g the evolution of α_s and of the running mass. Many choices are possible and we considered the following ones: $Q_W^2 = W \cdot W$, $\hat{s}$, s and $Q_g^2 = 4[m_c(m_c)]^2$, $g \cdot g$, $4m_D^2$.

The Structure Functions In principle, the parametrization of Eichten et al.[14] is best suited for our purpose, as it was fitted to neutrino data. However, given its usual failure when applied to low-energy physics, we shall consider several other possibilities. Notice that 'older' structure functions such as Owens-Reya can be legitimately used, as we are considering only light quarks at relatively low energies. To be consistent with perturbative QCD, we have to use the same scale Λ_{QCD} in α_s and in the structure functions, so that Owens-Reya ($\Lambda_{QCD} = 0.5$ GeV) gives the largest coupling and the largest result. It is debatable though whether charm production can still be considered a perturbative process at such high values of Λ_{QCD}.

The Implementation of Experimental Uncertainties First of all, the process is very dependent on the cut on muon momentum which puts a lower bound on the charm momentum. Because the cross section is a steeply falling function of this cut, smearing the muon momentum amounts to shifting it to a lower value. A shift of one standard deviation (9 GeV $\to$ 8.2 GeV) will be considered in the following.

One also has to take into account the fact that the parent neutrinos are not monoenergetic, and therefore once the cross section $\sigma(E_\nu)$ has been calculated (see Fig. 4), one must fold it with the incoming spectra (see Fig. 1). The net effect is to lower the high-energy part of the curve and raise the low-

energy one (see Fig. 5). As discussed above, the difference between the visible energy and the true parent neutrino energy is implemented by shifting the neutrino energy down by 12% after folding in the fluxes.

Estimate of the Theoretical Uncertainties Before drawing conclusions, we proceed to estimate an 'error' on these calculations. We do this by performing all possible calculations given the above-mentioned ambiguities. In Table I we tabulate the conclusion in terms of the factor increase in the quantity $\sigma(\mu^-\mu^-)/\sigma_{cc}$ resulting from exploiting each of these ambiguities. The largest calculation in this set is shown as the solid line in Fig. 5. It is obtained for Owens-Reya structure functions[14] (set 1), m_c given by Eq. (2.3) with $m_0 = 1.0$ GeV and all the parameters of Table I adjusted to maximize the result.

3.4 Results

Our suggestion to resolve the same-sign-dimuon puzzle is thus obvious. Other characteristics of the events are indeed compatible[5] with the predictions of the leading-order gluon-bremsstrahlung diagrams of Fig. 2. As for hadronic charm production only the normalization is a problem. We start by performing a straightforward calculation of the leading-order QCD diagrams. The result is shown in Fig. 4 for EHLQ structure functions.[14] We show two illustrative calculations. Both use a coupling constant running in the invariant mass of the gluon and their results are shown in Fig. 2. The upper curve also assumes a running mass of the charm quark given by Eq. (2.3) with $m_0 = 1.0$ GeV, $\Lambda_{\rm QCD} = 0.5$ GeV. The lower one assumes a fixed value $m_c = 1.25$ GeV.

Fig. 5 is obtained after smearing the cross section over the incoming fluxes and substituting the visible energy to the parent-neutrino energy. The results are then directly comparable to experiment. We conclude that theory and experiment are not inconsistent.

3.5 Conclusions

Although our estimates of the ambiguities are on the cautious or even pessimistic side, there is little doubt that the results span an order of magnitude (see Table I). Pinning down a more stable prediction will require higher-order calculations. These are difficult. One should also keep in mind that a non-perturbative contribution of the type discussed in the beginning could be present at some level. On the experimental side, one should also bear in mind that the data in Fig. 5 are obtained after subtraction of a large calculated background of muons from π, K-decay. In view of all this it could be argued that even a value of $m_c = 1.25$ GeV reconciles leading-order QCD with experiment as was already the case for hadroproduction. In fact, the disagreement between the calculation with $m_c = 1.25$ GeV and the data is less than two standard deviations. We give in Fig. 6 our prediction for cross sections extending to $E_\nu = 700$ GeV, from which one can get the ratio $\sigma_{\mu\mu}/\sigma_{cc}$ for any given experiment.

REFERENCES

1. F. Halzen, in *Proceedings of the 21st International Conference on High-Energy Physics*, Paris, 1982, edited by P. Petiau and M. Porneuf, J. Phys. (Paris) **43**, C3-381 (1982);
   C. Jarlskog, in *Proceedings of the Fourth Topical Workshop on Proton-Antiproton Collider Physics*, Bern, 1984, edited by H. Hänni and J. Schacher, CERN 84-09, p. 237.
   For earlier calculations, see:
   H. Goldberg, Phys. Rev. Lett. **39**, 1598 (1977);
   B.-L. Young, T. F. Walsh and T. C. Yang, Phys. Lett. **74B**, 111 (1978);
   G. L. Kane, J. Smith and J. A. M. Vermaseren, Phys. Rev. D **19**, 1978 (1979);
   K. Hagiwara, Nucl. Phys. **B173**, 487 (1980);
   S. J. Brodsky, C. Peterson and N. Sakai, Phys. Rev. D **23**, 2745 (1981).
2. A. Benvenuti *et al.*, Phys. Rev. Lett. **35**, 1199 (1975); Phys. Rev. Lett. **41**, 725 (1978);
   T. Trinko *et al.*, Phys. Rev. **D23**, 1889 (1981);
   M. Holder *et al.*, Phys. Lett. **70B**, 396 (1977);
   J. G. H. de Groot *et al.*, Phys. Lett. **86B**, 103 (1979);
   K. Nishikawa *et al.*, Phys. Rev. Lett. **46**, 1555 (1981); **54**, 1336(E) (1985);
   M. Jonker *et al.*, Phys. Lett. **107B**, 241 (1981).
3. H. C. Ballagh *et al.*, Phys. Rev. **D24**, 7 (1981);
   V. V. Ammosov *et al.*, Phys. Lett. **106B**, 151 (1981);

   A. Haatuft *et al.*, Nucl. Phys. **B222**, 365 (1983);
   P. Marage *et al.*, Z. Phys. C **21**, 307 (1984);
   C. Baltay *et al.*, Phys. Rev. Lett. **55**, 2543 (1985).
4. J.R. Cudell, F. Halzen and K. Hikasa, Phys. Lett. **B157**, 447 (1985).
5. H. Burkhardt *et al.*, 'Are There "Prompt" Like-Sign Dimuons?' preprint CERN-EP/85-191 (1985), submitted to Z. Phys. C.
6. S. Mishra, private communication.
7. R. M. Godbole and D. P. Roy, Z. Phys. C **22**, 39 (1984).
8. M. E. Duffy *et al.*, 'Characteristics of charm production by 400 GeV protons,' University of Wisconsin preprint WISC-EX-86-262 (1986).
9. D. Haidt, in *Proceedings of the 1981 International Symposium on Lepton and Photon Interactions at High Energies*, Bonn, edited by W. Pfeil (Bonn: Universität Bonn, 1981), p. 558.
10. S. J. Brodsky, J. C. Collins, S. D. Ellis, J. F. Gunion, and A. H. Mueller, in *Proceedings of the 1984 Summer Study on the Design and Utilization of the Superconducting Super Collider*, Snowmass, edited by R. Donaldson and J. G. Morfin (American Physical Society, 1984), p. 227.
11. V. Barger, W. Y. Keung and R. J. N. Phillips, Phys. Rev. **D25**, 1803 (1982).
12. C. Caso, in *Proceedings of the 1985 International Symposium on Lepton and Photon Interactions at High Energies*, Kyoto, edited by M. Konuma and K. Takahashi (Kyoto: Kyoto University, 1986), p. 488.

13. LEBC-EHS Collaboration, M. Aguilar-Benitez *et al.*, Phys. Lett. **161B**, 400 (1985).

14. J. F. Owens and E. Reya, Phys. Rev. **D17**, 3003 (1978);
M. Glück, E. Hoffmann and E. Reya, Z. Phys. C **13**, 119 (1982);
D. W. Duke and J. F. Owens, Phys. Rev. **D30**, 49 (1984);
E. Eichten, I. Hinchliffe, K. Lane and C. Quigg, Rev. Mod. Phys. **56**, 579 (1984).

Table I. Uncertainties in the calculation for the neutrino-induced same-sign-dimuon cross section.

Ambiguity in calculation at $E_\nu = 100$ GeV	Factor in $\sigma(\mu^-\mu^-)/\sigma(\mu^-)$
threshold parameter m_c ($1.01 \sim 1.65$ GeV)	10.5 ± 0.4
$\bar{z}$ of fragmentation $c \to D$ ($0.68 \sim 1.00$)	2.10 ± 0.08
scale of running coupling	1.47 ± 0.06
choice of structure function parametrization	1.26 ± 0.05
measurement error on cut p_μ ($8.2 \sim 9.0$ GeV)	1.25 ± 0.05
scale of structure functions	1.19 ± 0.05
contribution of s and b sea	≤ 1.07
$\xi \leq 10^{-3}$ part of the structure functions	≤ 1.03
parametrization of threshold behavior in α_s	≤ 1.02
details of charm decay, higher-order corrections...	?
cumulative factor	68 ± 15

FIGURE CAPTIONS

1. CDHS charged-current event rates, proportional to the parent-neutrino fluxes.
2. Leading-order QCD diagrams for the production of same-sign di-muons in ν-nucleon interactions.

3.a Soft, non-perturbative $c\bar{c}$ pair in the final-state quark jet in a regular charged-current ν-nucleon interaction.

3.b $c\bar{c}$ pair in final state quark jet in a soft (Pomeron P-exchange) nucleon-nucleon interactions.

4. The relative rate of same-sign dileptons to charged-current leptons are compared to the data of Ref. 5. It is calculated from the leading-order QCD diagrams of Fig. 2. For the lower two curves, the strong-coupling-constant scale is taken to be the gluon mass squared, the running-mass and the structure-function scales are taken to be the momentum transfer squared. The lower curve corresponds to a fixed mass $m_c = 1.25$ GeV, and the higher to a running mass with $m_0 = 1.0$ GeV. The highest curve is explained in the text.
5. Same as Fig. 4 after integration over the CDHS neutrino spectra for each bin (the curves are drawn to guide the eye).

6.a Same-sign-dilepton cross section from 100 to 700 GeV. The parametrization corresponds to that of Fig. 4.

6.b Charged-current cross section corresponding to Fig. 6.a.

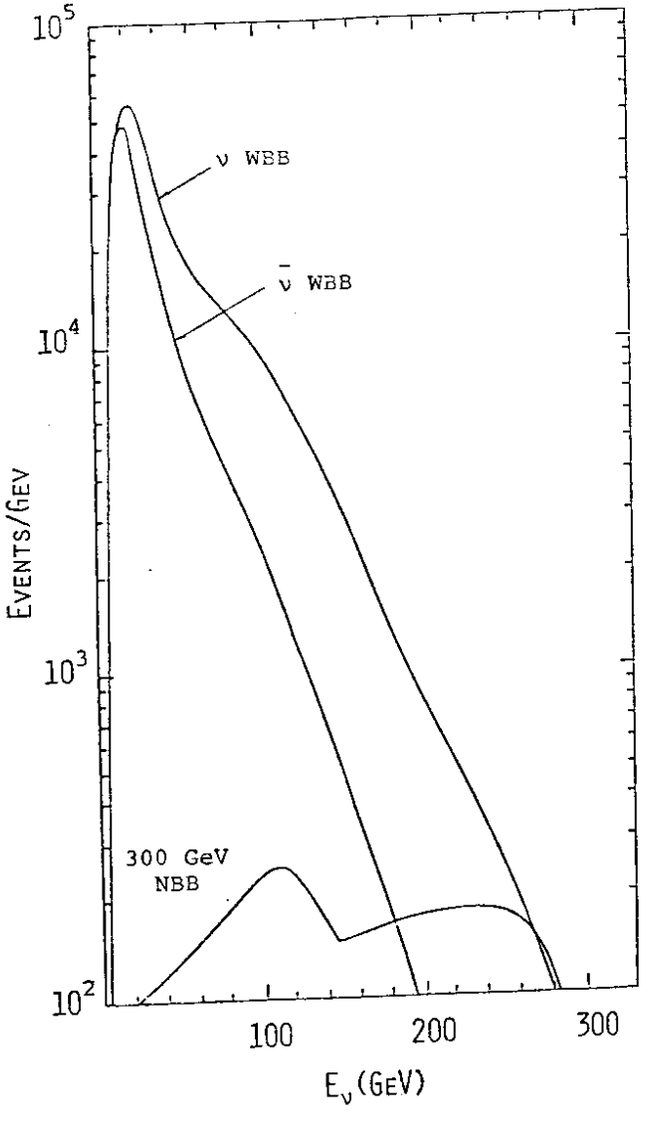

Figure 1

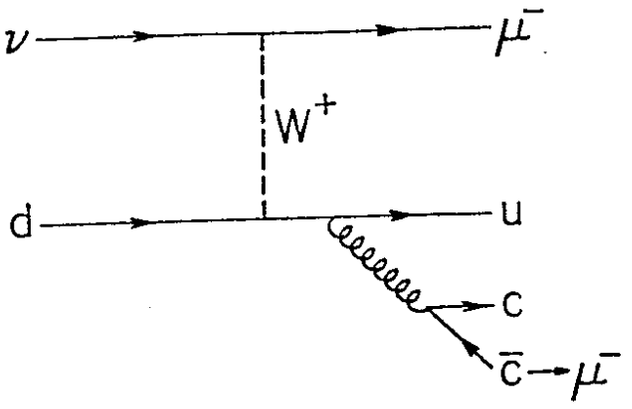

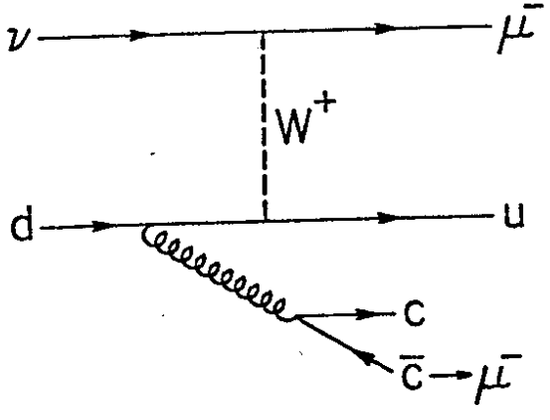

Figure 2

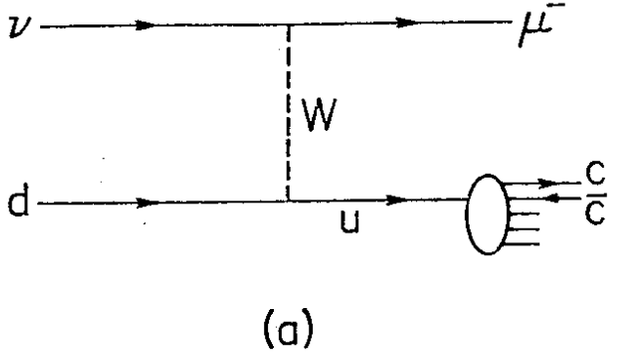

(a)

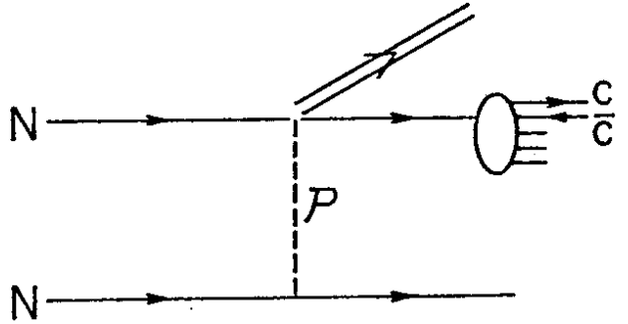

(b)

Figure 3.a and b

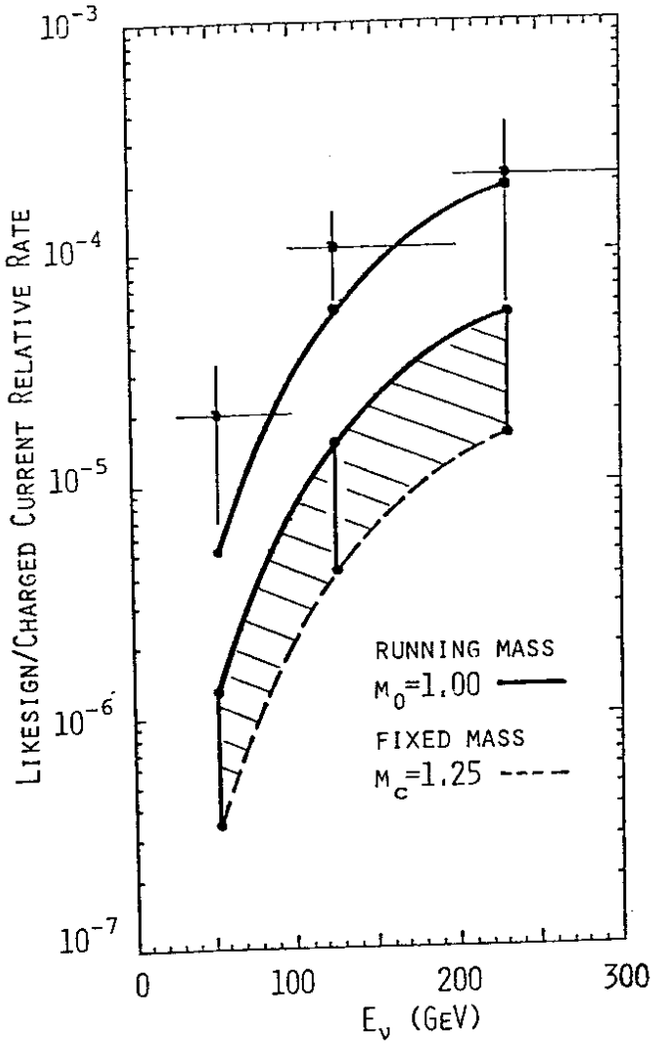

Figure 4

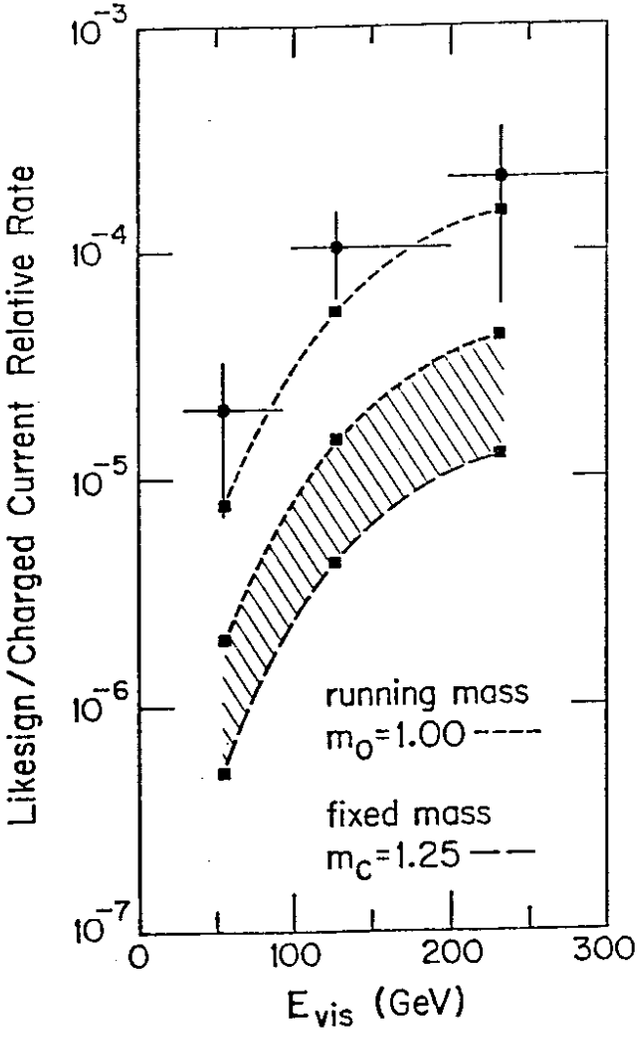

Figure 5

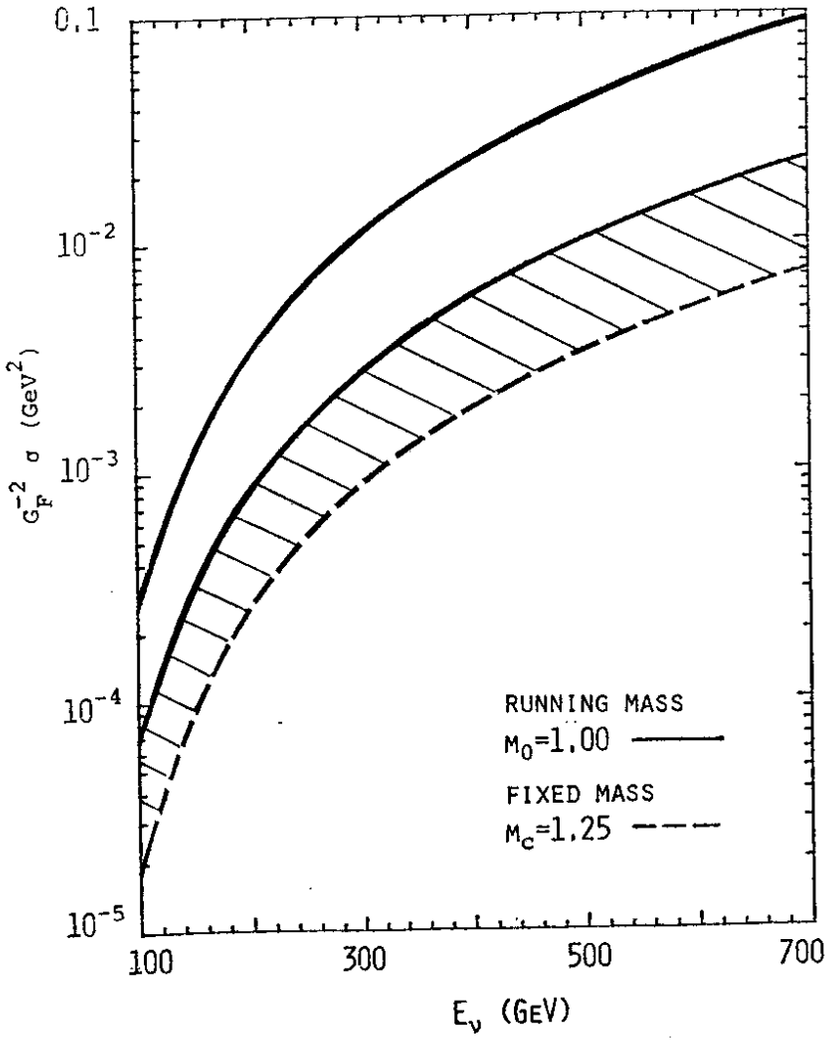

Figure 6.a

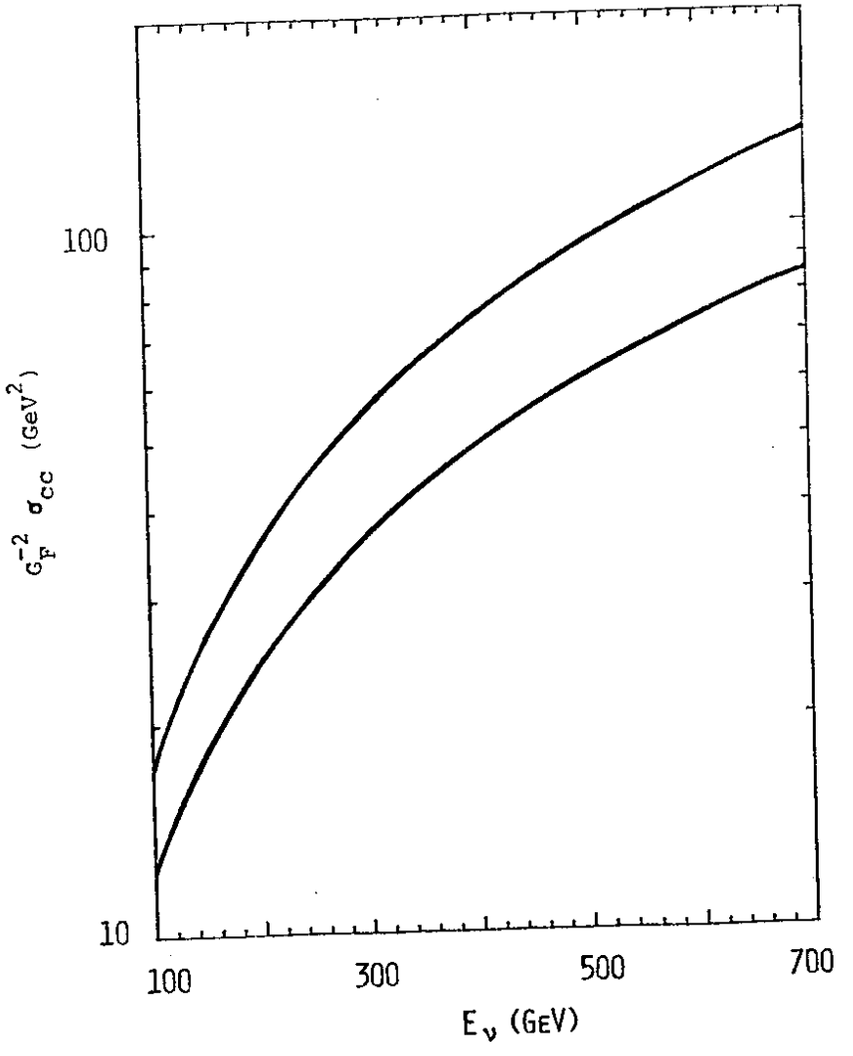

Figure 6.b

CHAPTER 4

The Cygnus X-3 Puzzle

4.1 Main Features of the Data

Several good reviews of the data exist[1] in the literature, so that we shall concentrate here on the most puzzling features of the signal(s) observed by roughly twenty underground and surface experiments and on the data relevant to our discussion rather than examine in detail all the experimental results.

Cygnus X-3 is a very powerful X-ray source discovered[2] in 1966 and confirmed in the early 70's by the *Uhuru* X-ray satellite. Since then, it has been observed in all regions of the electromagnetic spectrum, except in visible light which is blocked by galactic dust. The electromagnetic radiation has a period

$$T = 4.8 \text{ hours} \qquad (4.1.a)$$

which evolves at a rate

$$\frac{1}{T}\frac{dT}{dt} = 3.3\ 10^{-6}\ \text{yr}^{-1} \qquad (4.1.b)$$

The distance from Cygnus X-3 to Earth has been established from the absorption of its radio waves by interstellar hydrogen. Atomic H resonantly absorbs 23 cm wavelengths and the differential galactic rotation Doppler-shifts the absorption line from different parts of the galaxy. The width of

the resulting band enables one to determine the distance L from the object to Earth. The current lower bound is[3]:

$$L \gtrsim 10 \text{ kpc} \qquad (4.1.c)$$

and we shall use in the following 12 kpc as the most probable estimate.

The energy-differential flux of primary particles from Cygnus X-3 is given, for $E > 0.1$ TeV, by:

$$\frac{EdN}{dE} \approx 4 \times 10^{-16} \times \frac{E_{max}}{E}(\text{cm}^{-2}\text{s}^{-1}) \qquad (4.2)$$

where $E_{max} \approx 10^5$ TeV is the maximum observed energy. This number can be determined by counting the number of showers in the direction of Cygnus X-3 and estimating their energy. Notice however that the experiments do not detect the primary particle, but only its atmospheric cascade: they see the shower as a pancake of electromagnetic radiation 10^2 to 10^3 m^2 in area, a few nanoseconds thick and moving down the atmosphere at the speed of light. The nature of the primary must thus be inferred from the properties of the observed showers.

The Muon Rates The Kiel air shower array[4] group, after detecting a 4σ enhancement of the cosmic-ray flux in the direction of Cygnus X-3, analysed the particle content of the signal. They found a muon abundance $\sim$ 70% that of hadron showers. A qualitatively similar result has been found by Wdowczyk et al. for the Crab pulsar and more recently for Cygnus X-3 and

Hercules X-1 by the Los Alamos array. As we shall see later, such abundances are incompatible with standard particle physics.

Anomalous muon rates from point sources have also been observed by underground experiments[5]: whereas the expected underground muon flux from gamma-rays given by Eq. (4.2) is less than 10^{-13} cm^{-2}s^{-1}, SOUDAN I, situated at a depth of 2 km water equivalent, sees a muon flux of 7×10^{-11} cm^{-2}s^{-1} with a threshold energy $E_\mu^{min} = 0.65$ TeV, while NUSEX sees a flux $\approx 10^{-11}$ cm^{-2}s^{-1} at a depth of 4 km water-equivalent and with a threshold energy of 3.4 TeV. The muon threshold given here is the minimum energy that muons must have to reach the detector when produced in the atmosphere. In both cases the signal has the zenith-angle dependence characteristic of atmospheric cosmic-ray events. Notice that these fluxes are equal to the surface flux given by Eq. (4.2) for E=1 TeV, *i.e.* $\sqrt{s} = 43$ GeV.

Moreover, there seems to be a correlation between radio bursts and high-energy particles from Cygnus X-3. Haleakala and Baksan groups showed a correlation[6] between γ-rays with energies of 1 to 100 TeV and a radio burst of Cygnus X-3 in October 1985. Also SOUDAN I observed[7] excess muons during the radio flare. The IMB group has now utilized this correlation to re-analyse data from 1982 and 1984 and finds evidence[8] of excess muons at the time of the October 1983 outburst. Negative results from other experiments are at times or at observation depths where they are not in conflict with positive observations!

Notice also that neither NUSEX nor SOUDAN I see contained events originating from Cygnus X-3. This means that the muons have to be produced above the detector and that the lifetime and the cross section of the particles producing the signal must be adjusted to reduce appreciably their interactions or decays in the detector.

The Time Structure of the Signal The Kiel experiment checked that the on-source showers indeed remember the 4.8-hour binary period previously observed in X-ray and radio emissions, therefore confirming their origin. Kiel, Haleakala, Los Alamos and Baksan actually see a direct signal. All other experiments have to use the 4.8-hour periodicity of the signal in their analysis to extract a signal from Cygnus X-3 above the enormous cosmic-ray background (signal/background $\approx 10^{-2}$ at SOUDAN I and NUSEX). The data are submitted to a moment analysis where one assumes a periodic signal of period $T \equiv 4.8$ hours, so that the periodic signal is enhanced over the random background.

If one defines a phase $\phi = t/T$ with $\phi = 0$ corresponding to the X-ray minimum, the signal is observed by all experiments in either one or both of the phase intervals $[0.2, 0.3]$ and $[0.55, 0.75]$. The duration of the signal does not exceed $\sim 10\%$ of the period.

The Angular Spread of the Data Both NUSEX and SOUDAN I observe an angular spread of the data, *i.e.* although their angular resolution is $\sim 1^\circ$, the signal is maximum if they limit their analysis to the muons in a $3^\circ - 5^\circ$

cone around the direction of Cygnus X-3. The background is determined by looking at adjacent directions and extrapolating.

4.2 Model-Independent Constraints

Before embarking in a description of the source, we want to indicate what are the constraints on the primaries (which from now on we shall refer to as cygnets) that do not depend on any specific astrophysical model of the source.

Charge First of all, the cygnets must be neutral, otherwise they would interact with the intergalactic 3μGauss magnetic field and so lose all their direction and phase information: the 12 kiloparsecs distance from Cygnus X-3 to Earth represents more than 10^4 gyroradii for particles of energy $\sim 10^3$ TeV. Bare nuclei and protons are thus excluded as carriers.

Lifetime The cygnets must also be able to cover the 12 kpc distance without decaying. This means that the lifetime of a cygnet of energy E_C and mass M_C is:

$$\tau_{1/2} \gtrsim \frac{L}{\beta c \gamma} = 1.2 \times 10^9 \times \frac{M_C}{\sqrt{E_C^2 - M_C^2}} \text{ s} \qquad (4.3.a)$$

The case $M_C \ll E_C = E_{max} \approx 10^5$ TeV gives the shortest lifetime $\tau_{1/2}(\text{s}) \gtrsim 1.2 \times 10^4 \times M_C$ (GeV).

Size The galactic plane through which the cygnets go has a density $\rho_G \approx 1$ atom cm^{-3}, so that the column density seen by the cygnets is $z_G \approx 0.6$ g cm^{-2}. The interaction length is given by: λ_I (g cm^{-2}) $= \frac{1.66\times10^3}{\sigma\,(\text{mb})}$.

This means that to get here, the particles must have

$$\sigma \lesssim 2.7 \text{ b} \qquad (4.3.b)$$

This excludes atoms as possible carriers and limits the possibilities to nuclear and subnuclear particles.

Mass Mass limits can be derived from the pulsed nature of the observed signal. It is widely believed that the mass limits on cygnets are of order 1 GeV. We show[9] that these simple kinematic estimates are unreliable and can often be avoided. The actual mass limit depends critically on the detailed structure of the pulse, *i.e.* on (i) the shape of the flux as a function of energy and (ii) the minimum and maximum energies. We thus reconsider here the mass limits in detail.

Let us briefly review the original argument[1]: one assumes that the energy E of the muon parents is in the interval $E_{min}(\approx 10$ TeV$) \leq E \leq E_{max}(\approx 10^5$ TeV$)$. A particle of energy E and mass m has a velocity $\beta(E) = \frac{\sqrt{E^2-m^2}}{E} \approx 1 - \frac{m^2}{2E^2}$. The time interval between the arrival of particles of energies E_{min} and E_{max} is therefore:

$$\Delta t = \frac{L}{c}\left(\frac{1}{\beta(E_{min})} - \frac{1}{\beta(E_{max})}\right) \approx \frac{Lm^2}{2cE_{min}^2}\left(1 - \frac{E_{min}^2}{E_{max}^2}\right) \qquad (4.4)$$

where L is the distance to the star. The usual mass limit is obtained when one requires that all the particles arrive at Earth within a time small compared to the 4.8-hour period of the pulsed emission, *i.e.* $\tau \equiv \frac{Lm^2}{2cE_{min}^2} \approx \Delta t \leq 30$

min. For $L = 12$ kpc, one gets $m^2 \leq E_{min}^2 \times \frac{\Delta t}{6.18\ 10^{11}} \approx (0.54\ \text{GeV})^2$. Replacing the 30 minutes by the period of the system (4.8 hours) leads to the limit $m \lesssim 1.7$ GeV. Hence, this limit assumes that the pulse is totally concentrated within one period.

Actually, as we have mentioned above, the underground data have an enormous cosmic-ray background and only require that there be a pile-up of particles at a given arrival time. This can happen even if some of the (lower-energy) particles arrive at later times. Our argument can be intuitively understood as follows. Let us assume an incoming pulse of energy distribution $\frac{dN}{dE} = AE^n$ and let us divide the energy interval $[E_{min}, E_{max}]$ into four bins ($i = 1, 2, 3, 4$) of minimum energy $E_i = 10^i$ TeV and of maximum energy 10 E_i. The number of particles in the i$^{\text{th}}$ bin δN_i and the time interval δt_i within which they arrive are given by:

$$\begin{aligned} \delta N_i &\sim (10^i)^{n+1} \\ \delta t_i &\sim (10^i)^{-2} \end{aligned} \tag{4.5}$$

Hence the energy dependence of the flux is given by:

$$\frac{\delta N_i}{\delta t_i}(E_i) \sim 10^{i(n+3)} \tag{4.6}$$

So as long as $n > -3$, the in-time signal of the highest-energy particles will not be destroyed by the lower-energy ones arriving later, *i.e.* the lower-energy particles, although more numerous, are so spread out in time that they do not wash out the pulsed signal of the higher-energy particles arriving first. For example, in the case of an E^{-2} spectrum, particles with one tenth of

the maximum energy are 10 times more frequent but are spread out over a time interval 100 times larger, see Eq. (4.5). The high-energy part of the spectrum will be identified as the signal and the lower-energy part confused with the large background characteristic of present observations. The flux is still periodic in time. We have however to take into account the pile-up of particles from different periods and see how this affects the signal.

We therefore consider an explicit model of the pulsed emission. We assume that the star emits a flux of energy dependence E^n and of constant intensity during a fraction $\delta\phi$ of the period T:

$$\frac{dN}{dt^* dE} = A \sum_{j=-\infty}^{\infty} \theta(t^* - jT)\theta(\delta\phi - t^* + jT)E^n \tag{4.7}$$

with A a normalization constant. $\delta\phi$ can be thought of as the width of the signal in the phase plot at the source. The flux at Earth and the total beam energy are then given by:

$$\begin{aligned} \frac{dN}{dt} &= \frac{A}{n+1} \sum_{j=(1/T)(t-\delta\phi-\tau)}^{(1/T)(t-\tau E_{min}^2/E_{max}^2)} (E_b^{n+1} - E_a^{n+1}) \\ \frac{dE}{dt} &= \frac{A}{n+2} \sum_{j=(1/T)(t-\delta\phi-\tau)}^{(1/T)(t-\tau E_{min}^2/E_{max}^2)} (E_b^{n+2} - E_a^{n+2}) \end{aligned} \tag{4.8.a}$$

with $E_b = E_{max}$ if $t - jT \leq \delta\phi$, $E_b = \inf(E_{max}, E_{min}\sqrt{\frac{\tau}{t-jT-\delta\phi}})$ otherwise, $E_a = \sup(E_{min}, E_{min}\sqrt{\frac{\tau}{t-jT}})$ and $t = t^* - L/c$.

The width $\delta\phi$ has to be adjusted so that the half-width of the high-energy peak at Earth reproduces the observed 30 minutes. We take a typical value

$\delta\phi/T \approx 5\%$, with $T = 4.8$ hours. We consider values of n between -3 and -1 (-1 is the spectral index of γ-rays from monoenergetic pp collisions before cascading).

Some illustrative calculations are shown in Figs. 1 and 2 where we calculated the particle distribution dN/dt and the average cygnet energy

$$\langle E_C(t) \rangle = \frac{dN/dt}{dE/dt} \qquad (4.8.b)$$

Fig. 1 shows the well-known results for the case $m = 1$ GeV. Figs. 2.a and b give the results for $m = 100$ GeV and 1 TeV. One sees that if $n > -2$, these masses cannot be ruled out as we still obtain a pulsed signal. The peaks are no longer completely separated in time but experimental backgrounds prevent present experiments from observing this.

Notice that the flux of cygnets will not have an E^{-2} energy dependence if it is produced by a monochromatic beam and is not affected by the cascade (this would indeed be the case of a strongly interacting neutral particle). Also, the energy dependence of the cygnet flux should not be confused with the effective energy dependence of the muon flux experimentally observed: the latter results from the combined energy dependence of the cygnet flux at the source and of the cygnet interaction (or decay) length at Earth that determines the acceptance of the experiment. The width $\delta\phi$ over which the cygnets are emitted could also be much smaller than the phase width of the accompanying γ-rays if the particles are produced only in the last interaction length of the proton beam. One has indeed to assume that the width is

smaller than the one observed in the γ-ray spectrum, as it will be smeared on Earth by time retardation. We show in Fig. 3.a the effect of decreasing the width on the signal. One must have $0.05\ T \lesssim \delta\phi \lesssim 0.1\ T$ to reproduce the observed half-width of the pulses. The lowest cygnet energy E_{min} also has a big effect on the sharpness of the peak, as illustrated in Fig. 3.b for $n = -2$. Actually, if the cygnets were produced in a small-energy region, the mass limits previously given would drop altogether. The only way to achieve this would be to produce them in lepton-lepton collisions. As we shall see later, the standard astrophysical model of Cygnus X-3 disfavours this possibility.

Conclusion From the facts discussed above, cygnets have to be neutral particles of a mass smaller than 1 TeV and of a lifetime greater than 1.2 10^4 M_C(GeV) seconds. This rules out all known mesons and baryons, as well as atoms. One is then left with photons and neutrinos. As mentioned above, photon-initiated air showers have $\sim 2\%$ muons and thus cannot accomodate the Kiel results. Neutrinos, on the other hand, (i) would produce similar event rates at SOUDAN I and NUSEX and (ii) would not reproduce the zenith-angle dependence observed in both detectors. So no known particle can be the source of the observed signal.

Notice that the center-of-momentum energy reaches about 14 TeV, which is above the energy scale $\approx (\sqrt{2}\ G_F)^{-1/2} \simeq 0.25$ TeV where 'new physics' is expected in many models. One can indeed consider more exotic particles, such as those postulated by composite or supersymmetric theories. We shall

soon see that supersymmetry cannot provide a viable candidate for cygnets. The case of composite models has been considered without much success elsewhere[10] in the literature. Before evaluating the possible contributions from 'new physics', we need to introduce a picture of the Cygnus X-3 system and some basics of cascade theory.

4.3 The Standard Astrophysical Picture of Cygnus X-3

The Model The stability of the light curve and the magnitude of the period has led to a consensus that the periodic variations are produced by orbital motion in a binary system. The drop in the light curve would then correspond to the eclipse of the emitting star by the companion.

The 4.8-hour period of the system leads to the relation[11] (we shall use solar units from now on):

$$D = 1.4(M_s + M_p)^{1/3} \qquad (4.9.a)$$

where D is the distance between the centers of the two stars, M_s the companion-star mass and M_p the emitting-star mass. The duration of the eclipse (40% of the period) gives a relation for the companion-star radius R_s:

$$R_s = 0.95 \times D \qquad (4.9.b)$$

The energy dependence of the X-ray emission (*i.e.* from 10 keV to 2×10^6 MeV) is very similar to that of the Crab and Vela pulsars ;[12] therefore suggesting that one of the two objects is a neutron star. Notice that the

observation of a pulsar phase in gamma-ray data by the Durham group[13] has not been confirmed by any other experiment. Nevertheless, no other known type of source would produce the observed X-ray flux. If one of the stars is a stable pulsar, its mass M_p and radius R_p are constrained by[14]

$$\begin{aligned} R_p &\approx 10 \text{ km} \\ 0.15 \lesssim M_p &\lesssim 1.7 \end{aligned} \qquad (4.9.c)$$

As Eq. (4.9.b) shows, the companion star must be very close to the pulsar and will be disturbed by the gravitational interaction and by the particle emission from the pulsar. The X-ray eclipses are smooth, which suggests that the companion is not a compact object. If we assume that it is at least as big as a main-sequence star, and use the mass-radius relation for these stars, the condition $D \geq R_s$ leads to an upper bound[15]:

$$M_s \lesssim 4 \qquad (4.10)$$

Whenever an explicit model of the companion is needed, we shall use the parametrization of Gaisser and Stanev[16] which assumes a radius $M_s = 2.8$, $R_s = 2$ and a surface temperature of 10^4 K.

Gamma-Ray Production One now needs to explain how the intensity and the energy of the signal from Cygnus X-3 can be achieved. By analogy with the X-ray data, one assumes that the primaries getting to Earth are mainly photons. As pointed out by Vestrand and Eichler[15] the preceeding model can accomodate the production of 10^5 TeV gamma-rays: the idea is to use

the pulsar as an accelerator and the companion as a beam-dump. Then the process $pp \to (\pi_0 \to \gamma\gamma) + X$ is assumed to be the source of very-high-energy gamma-rays provided that the protons can be accelerated to $\sim 10^5$ TeV.

Indeed, if during gravitational collapse the magnetic flux is conserved, in the neutron-star phase the magnetic field would have grown as the inverse of the squared radius. For the Sun magnetic field ($B \approx 10$ Gauss), this would give a field $B \approx 10^{13}$ Gauss. If the ions are bound to the surface of the pulsar, this field can in principle produce a potential difference[17]

$$\Phi(\text{Volts}) \approx 6.6 \times 10^{12}\ P^{-2}(\text{s}^{-2})\ \text{B(TGauss)}\ \text{R}^3((10\ \text{km})^3) \qquad (4.11)$$

The companion star will be greatly disturbed by the close-by pulsar [see Eq. (4.9.b)] and is expected to eject protons in the pulsar direction. These protons would be accelerated by the field (4.11) to energies $\sim 10^5$ TeV. However, this intense electromagnetic field is unstable due to pair creation and it is not clear at all[17] that realistic models can produce such an acceleration.

We shall use the acceleration as input in a phenomenological model of gamma-ray production in Cygnus X-3 and show what the main characteristics of the accelerator should be. The simplest model was formulated by Hillas[18] and assumes that the pulsar produces a 10^5 TeV monochromatic proton beam replicating an accelerator. One can also use a generic cosmic-ray model where the proton beam has an E^n energy dependence. The intensity of the beam has to be enormous. The luminosity of the source can be

estimated in the following way:

$$I_C \approx F_O \times 4\pi\ L^2\ \frac{1}{D_\gamma}\ e^{R/\lambda_\gamma}\ \frac{1}{\epsilon_\gamma} \qquad (4.12)$$

where F_O is the observed flux [see Eq. (4.2)], *e.g.* $F_O = 10^{-10}$ ergs cm^{-2} s^{-1} above 1 PeV, L is the distance from Cygnus X-3 to Earth [see Eq. (4.1.c)], $D_\gamma \approx 0.1$ is the duty factor of the source, *i.e.* the fraction of the period during which the produced gamma-rays get to Earth or equivalently the time width of the pulses, $\epsilon_\gamma \approx 0.1$ is the ratio of the average photon energy to the parent-proton energy and λ_γ is the photon interaction length in the 3 K radiation background. This gives a total source intensity

$$I_C \approx 10^{39}\ \text{ergs s}^{-1} \qquad (4.13)$$

Notice that the gamma-rays below 1 PeV are produced as by-products of the atmospheric cascade in the star and their contribution is included in the factor ϵ_γ. I_C is to be compared with 5×10^{35} and 5×10^{33} ergs s^{-1} for the Crab and Vela pulsars respectively. The above estimate [Eq. (4.13)] can be significantly reduced if the beam is collimated (such as in the slot-gap acceleration model[17]), or if energetic gamma-rays are produced and can escape during the proton-acceleration process.

The Energy Crisis This enormous energy output leads to the instability[19] of the picture just described. The gravitational energy of the companion is $\sim \frac{G_N M_s^2}{R_s} \sim 4 \times 10^{48}$ ergs. The companion star will intercept 34% of that flux [see Eq. (4.9.b)] and so the ratio of the gravitational energy to the

intercepted energy will be $\sim 1.2 \times 10^{10}$ s, *i.e.* less than 400 years. Some of the radiation hitting the companion star will be radiated away, but about half of the neutrino flux resulting from $pp \rightarrow \pi^{+}_{-}$ will go deep into the star[20] and produce a heating $\sim 10^{37-38}$ ergs s^{-1}. This number is to be compared to the Eddington limit $F_E = 1.38 \times 10^{38} \times M_s$ ergs s^{-1}, which is the maximum power that can be produced at the center of the star without destroying it. In our case, although the flux from the pulsar is greater or equal to the Eddington limit, its effect on the companion star is not straightforward as the system does not have a spherical symmetry. Nevertheless, it is clear that the companion will be greatly disturbed by such an energy flux: the standard astrophysical picture of the system might indeed be inconsistent.

Moreover, considering cygnet emission makes the problem even much worse. The total energy emitted by the pulsar in cygnets is given by:

$$\left.\frac{dE}{dt}\right|_{tot} = \frac{F_\mu}{f_\mu} \langle E \rangle \ \frac{T}{\delta\phi} \tag{4.14}$$

where $F_\mu \approx 10^{36}$ s^{-1} is the total muon flux, f_μ is the muon multiplicity in cygnet interactions and $\delta\phi/T$ is the duty factor of the binary system. $\langle E \rangle$ is given by:

$$\langle E \rangle = \frac{n+1}{n+2} \frac{(E_{max}^{n+2} - E_{min}^{n+2})}{(E_{max}^{n+1} - E_{min}^{n+1})} \tag{4.15}$$

For $\delta\phi/T \approx 5\%$, $E_{min} = 10$ TeV, $E_{max} = 10^5$ TeV and $f_\mu \approx 1$, $n = -2.2$ gives a total energy output of 10^{39} ergs s^{-1}, which is the total proton flux in the Hillas model. For $n = 0$ we obtain 10^{42} ergs s^{-1}, which is the highest flux consistent with a Cygnus X-3 half-life (due to neutrino heating) of 10

years, assuming that 1% of the flux heats the companion.[20] These bounds are of course very loose as they depend strongly on the muon multiplicity and on the fraction of the flux going into neutrino heating of the companion. We also did not include the fact that Cygnus X-3 seems to be on only a fraction of the time;[21] so that the effective heating should be multiplied by 5% or less.

4.4 Simplified Cascade Theory

To address the particle-physics question of the muon abundances, we need one more ingredient. The production and detection mechanisms are cascade processes, *i.e.* processes through which a primary particle, after successive interactions with the medium and decays, produces a shower of secondaries. Given the fact that the primaries are extremely energetic, we shall assume that all secondaries are produced in the direction of the beam and thus reduce the problem to a one-dimensional one.

Main Equation of Linear Cascade Theory The generation of particles in the beam-dump is described by one-dimensional evolution of the particle flux[10]

$$\frac{dN_j}{dE_j dz} = -\frac{1}{\lambda_j}\frac{dN_j}{dE_j} + \sum_i \int_{E_j}^{Emax} \frac{1}{\lambda_i}\frac{dN_i}{dE_i}\frac{dN_{i\rightarrow j}}{dE_j}\, dE_i \tag{4.16}$$

The first term describes the depletion of the flux of particle j in the dump by interaction (or decay) while the second term accounts for the production of j by particle(s) i: z is the column density along the cascade direction and λ_k is the total evolution length of particle k combining the decay length $\lambda_{D,k}$

and the interaction length $\lambda_{I,k}$ ($1/\lambda_k = 1/\lambda_{D,k} + 1/\lambda_{I,k}$). One can rewrite:

$$\frac{dN_{i\to j}}{dE_j} = \frac{1}{\sigma_{i,total}} \times \frac{d\sigma_{i\to j}(E_i)}{dE_j} \qquad (4.17.a)$$

for interactions producing j and

$$\frac{dN_{i\to j}}{dE_j} = \frac{\lambda_i}{\lambda_{D,i}} \times \frac{D'(E_j/E_i)}{E_i} \times B_{ij} \qquad (4.17.b)$$

for decays, with B_{ij} the branching fraction for i to j and D' the fragmentation function $i \to j$. Eq. (4.16) becomes:

$$\begin{aligned}\frac{dN_j}{dE_j dz} = &-\frac{1}{\lambda_j}\frac{dN_j}{dE_j} \\ &+\sum_i \int_{E_j/E_{max}}^1 \frac{dN_i}{d(E_j/x_{ij})} \frac{\sigma_{i\to j}(E_j/x_{ij})}{1.66\times 10^3} D(x_{ij}) \frac{dx_{ij}}{x_{ij}} \\ &+\frac{1}{E_j}\sum_l \int_{E_j/E_{max}}^1 \frac{dN_l}{d(E_j/x_{lj})} D'(x_{lj}) \times B_{lj} \frac{M_l}{\tau_{1/2}\, c\, \rho} dx_{lj}\end{aligned} \qquad (4.18)$$

where we have assumed Feynman scaling, *i.e.* $\frac{d\sigma_{i\to j}(E_i)}{dE_j} = \frac{1}{E_i} D(x_{ij}) \times \sigma(E_i)$, with $x_{ij} = E_j/E_i$; ρ is the medium density in g cm^{-3}, $\tau_{1/2}$ is the lifetime of particle i and all the cross section are in mb. This formula allows for threshold behavior through the $\sigma_{i\to j}$ energy dependence. Notice that for the decay part we have assumed $E_i \gg M_i$.

Therefore in general one has a system of differential equations to solve. Several approximations can be introduced which greatly simplify the solution. First of all, the solution of the equation is trivial when one can neglect

the production terms:

$$\frac{dN_j}{dE_j} = \frac{dN_j}{dE_j}\Big|_{(z=0)} \times e^{-z/\lambda_j} \qquad (4.19)$$

Notice that this simple solution is rarely appropriate as usually the particle considered emits electromagnetic radiation and is thus its own parent (*e.g.* $p(=i) \to p(=j)\ \gamma$. This solution is valid only when one considers the most energetic particles, so that the lower-energy $j \leftarrow i$ can be neglected.

The Proton Beam The preceeding simple solution can be saved in the proton case. If one assumes that a power-law primary spectrum $\frac{dN_{i(=p)}}{dE_i} \sim E_i^{-K}$ and a constant proton cross section, one can see that assuming $\frac{dN_{j(=p)}}{dE_j} \sim E_j^{-K}$ leads to a solution:

$$\frac{dN_p}{dE_p dz} = -\frac{1}{\lambda_p} E_p{}^{-K} \times (1 + \int_0^1 x^{K-1} D(x)\, dx) \qquad (4.20)$$

which amounts to a modification of λ_j in Eq. (4.18).

The treatment of the proton beam in the Hillas model $\frac{dN_i}{dE_i} = N_i \delta(E_i - E_0)$ is less obvious. Rather than solving Eq. (4.16) exactly, one can use in first approximation the average solution $\frac{dN_j}{dE_i} \sim \langle N_j \rangle\, \delta(E_j - \frac{\langle E_j \rangle}{\langle N_j \rangle})$ with $\langle X \rangle \equiv \int_0^{E_{max}} X(E_j)\, dE_j$. One has, from Eq. (4.16) and for a constant λ_p:

$$\begin{aligned}\frac{d}{dz}\langle N_p \rangle &= \frac{1}{\lambda_p}\ \langle N_p \rangle \times (-1 + \int_0^1 \frac{dN_{i\to j}}{dx}\, dx) \\ &= \frac{1}{\lambda_p}\ \langle N_p \rangle \times (-1 + B_{p\to p}) \\ \frac{d}{dz}\langle E_p \rangle &= \frac{1}{\lambda_p}\ \langle E_p \rangle \times (-1 + \int_0^1 \frac{dN_{i\to j}}{dx}\, x\, dx)\end{aligned} \qquad (4.21)$$

We simplify further the picture by assuming that the branching $p \rightarrow p$ is equal to 1. This is a reasonable assumption as the baryonic number is conserved and as high-energy baryons will roughly have the same kind of interactions as high-energy protons. We further assume that the energy decays by a factor 2 after each effective interaction length which should be similar to the total interaction length.

Gamma-Ray Production and Detection Gamma-rays in Cygnus X-3 and in the Earth atmosphere have been the subject of numerous studies. In general, one has to solve a system of coupled differential equations[10] such as Eq. (4.18) or one can use Monte-Carlo methods[22] which allow for fluctuations. We shall only examine here the physics of the energy dependence of the produced gamma-ray flux. The simple picture that we have just developed reproduces Hillas's results[18] for gamma-rays. A monoenergetic pp collision produces gamma-rays with an energy spectrum $\sim 1/E_\gamma$. This power spectrum is stable during the cascade: the argument made for Eq. (4.20) holds true in this case, except that one gets a growing exponential factor due to the fact that the number of gamma-rays grows after each interaction length. We shall assume here for simplicity that the number of gamma-rays doubles after each interaction length and that the gamma-ray interaction length is comparable to that of the proton ($\lambda_\gamma \approx \lambda_p \equiv \lambda$). Notice that the maximum gamma-ray energy decreases by a factor 2 after each interaction length, so that for a gamma-ray of energy E to leave the star, the column density z must obey

$$\xi \equiv \frac{z}{\lambda} \leq \frac{\ln(E_0/E)}{\ln(2)} \equiv Z_{max} \qquad (4.22.a)$$

For a fixed ξ, the number of gamma-rays produced by the proton cascade is

$$\begin{aligned} \frac{dN}{dE}\Big|_\xi &= \frac{1}{E} \times \sum_0^\xi 2^{\xi - n} \\ &= \frac{1}{E} \times \frac{2^\xi - 2^{-1}}{1 - 2^{-1}} \end{aligned} \qquad (4.22.b)$$

where the sum is over all the proton energies and the n contribution comes from the fact that the proton cascade reduces the length of the gamma-ray cascade. All the gamma-rays of Eq. (4.22.b) have to be summed over the depth of the production layer. Each ξ has a probability $w(\xi)$ to be observed, proportional to the time during which it is viewed. One gets:

$$\begin{aligned} \frac{dN}{dE}\Big|_{total} &= \frac{1}{E} \times \int_0^{Z_{max}} d\xi \; w(\xi) \; \frac{2^\xi - 2^{-1}}{1 - 2^{-1}} \\ &= \frac{2}{\ln(2)\; E} \int_1^{E_0/E} dx \; w[\frac{\ln(x)}{\ln(2)}] \; \frac{x - 1/2}{x} \end{aligned} \qquad (4.22.c)$$

For $w(\xi)$ = constant, we see that Eq. (4.22.c) is steeper that an E^{-2} spectrum, and for $w(\xi) = 1/\xi$ (as in an exponential atmosphere[18]), a numerical integration of Eq. (4.22.c) gives a spectrum $\sim E^{-1.8}$. Notice that we have neglected the contribution of low-energy proton secondaries such as pions, which should steepen the flux. Hence a monochromatic proton beam produces an $\sim E^{-2}$ gamma-ray spectrum through the cascading process.

Finally, one has to realize that the gamma-ray production rate depends heavily on the model of the star used. Eq. (4.22.a) gives the maximum column density for gamma-ray production but the relation between that density and the phase-width of gamma-rays (and thus the duty cycle of the accelerator) is model-dependent.

Once they reach the Earth atmosphere, these gamma-rays start another shower through e^+e^- pair creation and bremstrahlung. Muon production is heavily suppressed[10] and the muon content of gamma-ray showers is expected to be $\sim 2\%$ that of hadron showers, contradicting the Kiel experiment which sees $\sim 70\%$.

Neutrino Production As protons emit gamma-rays through the process $pp \rightarrow (\pi_0 \rightarrow \gamma\gamma) + X$, they also produce neutrinos through $pp \rightarrow (\pi^{\pm} \rightarrow \nu) + X$. Physical consequences of neutrino emission are twofold: (i)neutrinos can produce muons at Earth, so that an estimate of the neutrino background is crucial to the interpretation of the data and (ii) neutrinos interact with the core of the star and could destabilize it through heating. This calculation, well documented[23] in the literature, is very similar to the photino production that we are about to evaluate, so that we are going to point out several interesting physical facts relevant to the following argument.

The lifetime of the charged pions is very long ($\tau_\pi \approx 2.6 \times 10^{-8}$ s) , so that one will have a competition between decay into neutrinos and interactions. At very high energies, due to time dilation of the pion lifetime [see Eq. (4.18)], the interactions will win, so that the most energetic neutrinos from pions will be suppressed. The heating will surprisingly come from the enormous number of low-energy neutrinos produced through $\pi p \rightarrow (\pi \rightarrow \nu) + X$. Processes with much smaller cross sections such as Λ_c or gluino production, for which the lifetime is much smaller, will add an appreciable fraction to the heating from pion neutrinos as decays will compete much less with interactions.

The neutrino fluxes are comparable to the photon fluxes[16] and the neutrino contribution to underground muon production is $\sim 10\%$ that of photons.

The calculation of neutrino heating and fluxes is not very sensitive to the astrophysics parameters or to the cascade picture. Once produced, neutrino fluxes are very insensitive to the depth of the matter they encounter and the proton cascade will be essentially model-independent in the bulk of the star.

The initial structure of the beam is not overly important as by cascading the energy will span the whole range from the maximum proton energy to the neutrino energy. For instance, in our simplified picture of the Hillas model, the number of protons between E and $2E$ is constant, so that $dN_p/d\ln(E)$ is constant, *i.e.* the proton beam is equivalent to a $1/E$ beam going through one interaction layer. Only atmospheric contributions are very model-dependent, but in the neutrino case, these are an order of magnitude smaller than the bulk contributions.

4.5 Supersymmetric Particle Production

Many authors[10,24] have considered the emission of light stable supersymmetric particles, photinos or gluinos, by cosmic accelerators such as Cygnus X-3. Previous calculations were approximate and incomplete as only production in the atmosphere of the main-sequence star was taken into account. As the particle-physics parameters are uncertain in the problem under consideration it is adequate to limit ourselves[25] to our simple picture of the Hillas model[18] when particle production occurs in the bulk of the star. We

will consider alternative models of the beam when the main contribution comes from the atmosphere of the companion star.

Particle Physics Assumptions We first need to specify the processes involving supersymmetric particles in the beam-dump. Supersymmetry predicts that a new multiplicative quantum number, R-parity, is conserved. This implies that superparticles are produced in pairs and that one of them is stable. Whereas the masses must be ~ 1 TeV or less, the actual values are not predicted. Anticipating small effects in general, we concentrate on scenarios which maximize observable fluxes. We consider the simplest $N = 1$ supergravity where all scalar quarks have a common mass $m_{\tilde{q}}$ and the gauginos are not mixed.[26] If masses originate from radiative corrections the photino is the most natural candidate for the lightest, stable superparticle. Photino fluxes will result from the production and decay of gluinos and squarks in the dump. Gluino production cross sections exceed those of squarks of a similar mass. Furthermore, as present mass limits are less stringent for gluinos, we assume that they are the dominant source of photinos via the decay $\tilde{g} \to \tilde{\gamma} q \bar{q}$. Subsequently we will also discuss the possibility that the $\tilde{g}$, rather than the $\tilde{\gamma}$, be stable.

Cascade and Heating in the Photino Case At each phase angle ϕ we perform a cascade calculation neglecting secondary interactions except for those of the protons and superparticles themselves. The proton secondaries, such as pions, will be very soft and can be ignored due to the threshold behavior of the production cross sections. For the secondary protons we adopt the

simple cascade model developed above, where the number of protons is constant and the proton energy is reduced by a factor 2 for every interaction length λ_p, with

$$\lambda_p(\mathrm{g/cm^2}) = \frac{1.66 \times 10^3}{\sigma_{\mathrm{tot}}(\mathrm{mb})} \tag{4.23}$$

and

$$\sigma_{\mathrm{tot}}(\mathrm{mb}) = 38.5 + 4.3 \ln^2 \left(\frac{s}{100\ \mathrm{GeV}^2} \right) \tag{4.24}$$

For each interaction length we subsequently calculate the number of produced gluinos[27] per incident proton, with

$$\frac{dN_{\tilde{g}}}{dE} \simeq \frac{2}{\sigma_{\mathrm{tot}}} \frac{d\sigma_{p \to \tilde{g}}}{dE} \tag{4.25}$$

The gluinos decay into stable photinos or interact. The decay $\tilde{g} \to \tilde{\gamma} q \bar{q}$ is again calculated[28] in the collinear approximation. If they do not decay the gluinos are dressed into gluino-hadrons which re-interact in the target with hadronic-size cross sections

$$\sigma_{\tilde{g}p} \simeq 10 - 10^2\ \mathrm{mb} \tag{4.26}$$

Explicit calculations are not very sensitive to the exact value. We will perform computations assuming a 10 mb cross section. The γ-flux after $(i-1)$ interaction lengths is given by

$$\left. \frac{dN_{\tilde{\gamma}}}{d \ln E} \right|_i = \int_{-\infty}^{0} d \ln x_{\tilde{g}} \, \frac{d\sigma_{p \to \tilde{g}}}{d \ln x_{\tilde{g}}} \, D_{\tilde{g} \to \tilde{\gamma}} \left(\frac{x_{\tilde{\gamma}}}{x_{\tilde{g}}} \right) \frac{x_{\tilde{\gamma}}}{x_{\tilde{g}}} \, f \, \theta \left(\frac{x_{\tilde{\gamma}}}{x_{\tilde{g}}} - \frac{m_{\tilde{\gamma}}^2}{m_{\tilde{g}}^2} \right) \tag{4.27}$$

Here $x_{\tilde{g}} = E_{\tilde{g}}/E_p$, $x_{\tilde{\gamma}} = E_{\tilde{\gamma}}/E_p$ with $E_p = (10^5\ \mathrm{TeV})/2^{(i-1)}$. $D_{\tilde{g} \to \tilde{\gamma}}$ describes the gluino decay in the collinear approximation[28] and the fraction f takes

into account the competition between gluino decay and interaction

$$f = \frac{\lambda_I}{\lambda_I + \lambda_D} \tag{4.28.a}$$

with:

$$\lambda_I(\mathrm{cm}) = \frac{1.66 \times 10^3}{\sigma_{\tilde{g}p}(\mathrm{mb})\rho(\mathrm{g/cm^3})} \tag{4.28.b}$$

and

$$\lambda_D(\mathrm{cm}) = 5.35\ 10^{-12}\ \frac{E_{\tilde{g}}(\mathrm{GeV})}{\Gamma_{\tilde{g}}(\mathrm{GeV}) m_{\tilde{g}}(\mathrm{GeV})} \tag{4.28.c}$$

This approximation is derived using the same assumption as for Eq. (4.19) but should be much better than in the proton case. The cross section used here corresponds to the 'hard' part of the gluino-hadron total cross section for which the gluino-hadron is totally disturbed and produces many secondaries, so that the resulting supersymmetric secondaries are much softer than the gluino-hadron and can be neglected. Moreover, the interaction contribution to f is always very small as the gluinos are very unstable, so that the calculation is very insensitive to the way gluino interactions are treated.

As, unlike previous calculations, we take into account the full body of the star as well as its atmosphere, we also have to evaluate the photino interaction after production. The cross section $\sigma_{\tilde{\gamma}p}$ is obtained from the dominant process $\tilde{\gamma}q \rightarrow \tilde{g}q$ which has been evaluated taking fully into account the width and the propagator of the exchanged scalar quark (see Appendix B).

The final photino flux emitted by the binary is

$$\frac{dN_{\tilde{\gamma}}}{d\ln E} = \sum_i \left.\frac{dN_{\tilde{\gamma}}}{d\ln E}\right|_i \exp\left(-\frac{z_i}{\lambda_{\tilde{\gamma}}}\right) \tag{4.29.a}$$

where

$$\lambda_{\tilde{\gamma}}(\mathrm{g/cm^2}) = \frac{1.66 \times 10^3}{\sigma_{\tilde{\gamma}p}(\mathrm{mb})} \tag{4.29.b}$$

and

$$z_i = z - \sum_{j<i} \lambda_p \left(\frac{E_0}{2^{j-1}}\right) \tag{4.29.c}$$

One can also extract from (4.29.a) the $\tilde{\gamma}$-flux absorbed in the target-star by the substitution

$$\exp\left(-\frac{z_i}{\lambda_{\tilde{\gamma}}}\right) \longrightarrow 1 - \exp\left(-\frac{z_i}{\lambda_{\tilde{\gamma}}}\right) \tag{4.30}$$

Results and Conclusions For reasons previously discussed we first investigate models with

$$m_{\tilde{\gamma}} < m_{\tilde{g}} < m_{\tilde{q}} \tag{4.31}$$

Although we have done a rather exhaustive study we will illustrate the results with two examples

$$\begin{aligned} &\text{(I)} \quad m_{\tilde{g}} = 3\ \mathrm{GeV}, \quad m_{\tilde{q}} = 300\ \mathrm{GeV} \\ &\qquad\ \ m_{\tilde{g}} = 7\ \mathrm{GeV}, \quad m_{\tilde{q}} = 100\ \mathrm{GeV} \\ &\text{(II)} \quad m_{\tilde{g}} = 60\ \mathrm{GeV}, \quad m_{\tilde{q}} = 600\ \mathrm{GeV} \end{aligned} \tag{4.32}$$

In each case the photino is light, we show calculations for $m_{\tilde{\gamma}} = \frac{1}{6} m_{\tilde{g}}$. The results are essentially the same for a massless photino. Case (I) illustrates the 'window of opportunity' for light supersymmetric particles, *i.e.* the low-mass range not closed at present by accelerator limits. Notice that for a gluino mass as light as 3 GeV we have to increase the squark mass[29] to be compatible with accelerator limits. Example (II) illustrates a scenario of 'realistic' masses not yet within reach of accelerator experiments.

Results for fluxes are shown in Figs. 4 and 5 as functions of energy and binary phase angle. As can be seen from Fig. 4, the photino fluxes at Earth are small compared to photon and neutrino fluxes obtained within the same framework. At the higher energies the $\tilde{\gamma}$ fluxes become a few percent of the γ flux for models of type (I). It is likely that we underestimated the $\tilde{\gamma}$ fluxes as in this case the production cross section of the relatively light parent gluinos could be underestimated by a leading-order perturbative calculation. This is a familiar issue in connection with the hadronic production of charm. Models of type (I) are within reach of the new generation of cosmic-ray telescopes especially as the event signatures for detecting the admixture of photinos in the photon flux are promising. This has been discussed elsewhere.[24] It is however also very clear from these illustrative calculations that supersymmetric particles are not the source of the underground muons from Cygnus X-3 reported by some experiments.[30,31] Whatever the details of the signature produced at Earth, the event rate in underground detectors will be relatively small and definitely unobservable with present detectors.

In Fig. 6 we show the gluino flux from Cygnus X-3 assuming that the gluinos themselves are stable and reach Earth. Results are shown for $m_{\tilde{g}} = 3$ and 7 GeV. They qualitatively agree with a calculation from Ref. 1, which was done for a E^{-2} pulsar-beam spectrum and did not take into account the details of the companion atmosphere. Notice however that an E^{-2} flux predicts enhanced gluino production as one more readily samples low-energy processes where the cross section is enhanced: as expected, the atmospheric calculation is model-dependent. Even here the fluxes are in general small. The gluinos will interact with the atmosphere very much the way regular hadrons do. They will therefore produce roughly 10^2 times[32] more underground muons than photons do. As the flux in Fig. 6 is however suppressed by a factor $10^3 \sim 10^5$ we expect a muon rate of 10% or less of the rate generated by photons. Again, such rates might be observable in future experiment but exclude stable gluinos as a source of the muons reported in Ref. 5.

The previous calculation illustrates how results can be sensitive to the details of the beam. This is however not the case for the stable $\tilde{\gamma}$ calculations where the main contribution to the flux comes from the core of the target star. Results are only sensitive to the total luminosity of the beam. This discussion brings us naturally to the issue of heating of the companion by photinos deposited in the core. The discussion is completely parallel to that of heating by neutrinos.[20] Results are obtained from Eqs. (4.9)-(4.12) and shown in Table I. From the particle-physics point of view the crucial ingredients in the calculation are the $\tilde{\gamma}$ interaction cross sections with matter. They are shown in Fig. 7 where they are compared with the corresponding

cross section for conventional neutrinos. We estimate that the heating is at most $\sim 20\%$ of that due to neutrinos.[20]

As previously pointed out these results should be rather independent of the details of the binary system. The crucial astronomical input is the luminosity of the beam. It is important to remember at this point that the 'measured' luminosity of 10^{39} ergs/s represents a lower limit. A case for boosting it has been made in connection with the puzzling observation of underground muons. A corresponding boost in flux will result for neutrinos and supersymmetric particles, but not necessarily for photons. The latter could be suppressed by adjusting the beam-dump density. One does not have total freedom as the increased flux eventually destabilizes[20] the companion star by heating. The fact that binaries are stable represents a constraint on high-energy-particle-physics processes, independent from any direct observations.

4.6 Conclusions and Comments

As we mentioned before, the standard model cannot accomodate the observed muon rates of cygnet showers, without mentioning the angular spread of the data and the decay of the signal with depth. We just saw that supersymmetry does not solve this problem either, at least when supersymmetric particles are produced in pp collisions within the companion star. Other more exotic possibilities have been considered[1] but no viable explanation has been offered.

Model We shall here give the general features of a model inspired by Ruddick.[33] The basic idea of the model is to produce muons via the reaction $Cp \to (C' \to \mu^+\mu^-) + X$. The intermediate C' carries only a fraction f of the cygnet energy. The angular spread of the muons $\delta\theta_\mu$ is then given by

$$\sin(\delta\theta_\mu) = M_{C'}/(fE_C) \tag{4.33}$$

with $E_C = \langle E_C(t)\rangle$ [see Eq. (4.8.b)]. We give in Fig. 8 the time-dependent angular spread we get for $f = 1\%$ and $M_{C'} \approx M_C = 0.1 - 1.0$ TeV. We see that a spread of 3° can be achieved for $n > -2$.

This angular spread can actually be used to loosen the mass limits previously established: the background particles arriving at later times will have lower energies and therefore a higher angular spread: closing down the angle around the source should increase the signal-to-background ratio. We give our estimate of the signal-to-background ratio in Table II. We concentrate on the first tenth of the period and define the background as

$$B = \frac{1}{9}\int_{0.1T}^{T} dt \frac{dN}{dt} \tag{4.34.a}$$

and the signal as

$$S = \int_0^{0.1T} dt \frac{dN}{dt} - B \tag{4.34.b}$$

If we limit our background calculation to the fraction of muons arriving within a 3° cone, the mass limits are further weakened and masses ~ 1 TeV are allowed even for an E^{-2} cygnet spectrum. One would also expect the

experimental background to go up during periods of high activity such as radio bursts, as this background is determined by looking at the region of the sky around the source direction, which should contain a sizeable fraction of muons from the low-energy part of the cygnet pulses.

One can characterize rather precisely the particles involved in this two-step process. First of all, the original cygnets, already constrained by Eqs. (4.3.a) and (4.3.b), are presumably the source of the muon abundance at Kiel. This means that they must interact in the atmosphere ($z_{atm} \approx 1000$ g cm^{-2}), so that

$$\sigma_C \gtrsim \frac{2.4 \times 10^4}{z_{atm}}(\text{mb}) \gtrsim 24 \text{ mb} \qquad (4.35.a)$$

At the energy scale under consideration, it is likely that they will interact with the quarks inside the nucleon, hence providing a natural explanation of the scale f needed to explain the angular smear of Eq. (4.33). If they interact with nuclei, they will also produce a hadron shower. So one needs a cygnet flux $\sim 70\%$ of the total flux (see Section 1) to explain the Kiel muons. The cygnets at the source won't go through more than a few 1000 g cm^{-2} of matter, so that they will be confined to the atmosphere of the star and the width of the signal will be

$$\delta\phi/T \approx 10^{-2} \qquad (4.35.b)$$

This means that a big mass $O(100$ GeV) or more will actually be needed to explain the time width of the signal at Earth.

One can then characterize the secondaries. The lifetime can be estimated from the fact that they reach NUSEX after being produced in the atmosphere. If we impose that they have to travel ~ 1 km, we get the estimate

$$\tau_{C'} \gtrsim 3 \times 10^{-9} \text{ s} \qquad (4.36.a)$$

As this lifetime is long, we can estimate easily the ratio of contained events to penetrating ones by assuming that the number of particles remains constant in the vicinity of the detector. One gets for a cubic detector in a $3-5°$ cone:

$$\frac{\text{number of contained events}}{\text{number of events}} \approx \tan(\frac{3-5°}{2}) \approx 2-5\% \qquad (4.36.b)$$

Given the low statistics of the experiment, this predicts ~ 1 event which is consistent with a negative observation.

One can now estimate the interaction cross section of C' with nuclei A. The signal is damped by a factor ~ 10 when one goes from SOUDAN I to NUSEX. The total interaction length[33] $\lambda_{C'} = (1/\lambda_I + 1/\lambda_D)^{-1}$ must be $\sim 1-2 \times 10^5$ g cm^{-2}, and assuming that $\lambda_D \approx z_{NUSEX}$ leads to:

$$\sigma_{C'A} = 0.5 - 1 \ \mu\text{b} \qquad (4.36.c)$$

The problem arises when one calculates the C' flux needed to produce the observed underground data. The number of C' that interact or decay is given

by:

$$N = N_0\, e^{-z_d/\lambda_{C'}} \times (1 - e^{-z_{max}/\lambda_{C'}}) \approx N_0\, e^{-z_d/\lambda_{C'}} \times (\frac{z_{max}}{\lambda_{C'}}) \quad (4.37)$$

where z_{max} is the maximum column density away from the detector that would still produce the observed $3-5°$ angular spread of the data and z_d is the detector depth. For a density $\rho \approx 3.3$ g cm^{-3} and a detector size ~ 3.5 meters, one gets $z_{max} \approx 250 - 440$ g cm^{-2}. The fraction that will decay and thus actually produce an angular smear is given by Eq. (4.28.a) and for the above parameters is ~ 6 to 40 %. For the observed fluxes, the total number of C' at ground level is then:

$$4 \times 10^{-8} \gtrsim N_0 \gtrsim 9 \times 10^{-10} \quad (4.38)$$

This clearly violates the earlier estimate based on surface experiments.

One could conceive a few ways out of this problem: the original idea is to make the process a low-energy one, so that the primary particle flux would be higher. One has however to go down to energies $O(100$ GeV) and to smaller masses, and it is difficult to imagine that such an anomalous behavior could have been missed in accelerator experiments. One could also reduce the primary C cross section, so that it would produce fewer surface muons and the flux could be increased without contradicting surface experiments. The increase of the flux should however be enormous ($\sim 10^4$) and astrophysics seems totally unable to produce a semi-stable binary system under such conditions.

Other Alternatives One can systematically classify the possible ways out of this challenge:

- One can neglect part of the data and make a model à la Ruddick. All the experimental evidence is very loose, so that it is hard to tell what has to be excluded from the analysis.
- If one believes in the basic features of the astrophysical picture of the binary, we have seen that it is very hard to produce a sizeable amount of particles from the energy region where new physics is expected. One has then to re-evaluate[34] the way one does the cascade calculation in the Earth atmosphere. As photon interactions are very constrained by QED measurements, one has to consider the possibility of collective effects in high-energy cascades.
- One can finally reject the astrophysical picture and consider more exotic stars, made *e.g.* of quark matter![35]
- We want to emphasize here the fact that the acceleration mechanism is not known, that the apparent correlation between the underground muons and the radio bursts is hardly understood and that the 'new physics' contributions to stellar collapse have not been evaluated, to the best of our knowledge.

REFERENCES

1. For a complete review, see A.A. Watson, rapporteur paper in *Proceedings of the* 19^{th} *International Cosmic-Ray Conference*, La Jolla, 1985 (Washington D.C.: NASA, 1985).
   See also J. Learned, University of Hawaii Internal Report (unpublished), 1985;
   J.W. Elbert, R.C. Lamb and T.C. Weeks in *Proceedings of New Particles '85*, Madison, Wisconsin, edited by V. Barger, D. Cline and F. Halzen (Singapore: World Scientific, 1986);
   B.M. Vladimirskii, A.M. Gal'per, B.I. Luchkov and A.A. Stepanyan, Sup. Riz. Nauk. **145**, 255 [Sov. Phys. Usp. **28**, 153 (1985)];
   F. Halzen, CERN TH.4570/86 and SLAC 1986 Summer Institute on Particle Physics, edited by E. Brennan.
2. R. Giacconi, P. Gorenstein, H. Gursky and J.R. Waters, Ap. J. **148**, L119 (1967);
   R. Giacconi, E. Kellog, P. Gorenstein, H. Gursky and H. Tannanbaum, Ap. J. **165**, L27 (1971);
   C. Leong, E. Kellog, H. Gursky, H. Tannanbaum and R. Giacconi, Ap. J. **170**, L67 (1971).
3. L.L.E. Braes and G.K. Miley, Nature **237**, 506 (1972);
   T.C. Weekes, H.P. Murphy, R. Schild, H. Gursky, J. Geary and T. Stephenson, Publ. Astron. Soc. Pacific **93**, 474 (1981);
   J.M. Dickey, Ap. J. **273**, L71 (1983).

4. M. Samorski and W. Stamm, Ap. J. **268**, L17 (1983); T. Dzikowski *et al.*, in *Proceedings of the* 19^{th} *International Cosmic-Ray Conference*, La Jolla, 1985 (Washington D.C.: NASA, 1985);
   G. Yodh, *Telemark IV*, Ashland, 1987.
5. J. Bartelt *et al.*, (Soudan I Collaboration), Phys. Rev. **D32**, 1630 (1985);
   M.L. Marshak *et al.*, Phys. Rev. Lett. **54**, 2079 (1985); **55**, 1965 (1985);
   G. Battistoni *et al.*, (NUSEX Collaboration), Phys. Lett. **155B**, 465 (1985);
   C. Berger (Frejus Collaboration), in *Proceedings of the International Europhysics Conference on High-Energy Physics*, Bari, Italy, 1985 (to be published).
   See, however, E. Aprile *et al.*, (HPW Collaboration), in *Proceedings of the International Europhysics Conference on High-Energy Physics*, Bari, Italy, 1985 (to be published);
   Y. Oyama *et al.*, (KAMIOKANDE Collaboration), University of Tokyo preprint UT-ICEPP-85-03 (1985).
   See also L.E. Price, Argonne preprint ANL-HEP-CP-85-117, in *Proceedings of Annual Meeting of the Division of Particles and Fields of the American Physical Society*, Eugene, 1985, edited by R.C. Hwa (Singapore: World Scientific, 1986);
   Y. Totsuka, University of Tokyo preprint UT-ICEPP-85-05 (1985), in *Proceedings of 1985 International Symposium on Lepton and Photon Interactions at High Energies*, Kyoto (to be published).

6. HGO collaboration, in *Proceedings of the 1986 Durham Workshop on Gamma-Ray Astronomy*, edited by T. Turver;
V.V. Alexeenko and A.E. Chudakov, European Cosmic-Ray Symposium, Bordeaux, France (1986).
7. M. Marshak, in *Proceedings of the XXIII International Conference on High-Energy Physics*, Berkeley (1986) (to be published).
8. IMB Collaboration, submitted to Phys. Rev. D (1986).
9. J.R. Cudell, F. Halzen and P. Hoyer, Madison Preprint MAD-PH-339 (1987).
10. F. Halzen, K. Hikasa and T. Stanev, Phys. Rev. **D34**, 2061 (1986) and references therein.
11. H. Gursky and E. Schreier, in Neutron Stars, Black Holes and Binary X-Ray Sources, edited by H. Gursky and R. Ruffini (Boston: D. Reidel Publishing Company, 1975).
12. M. Milgrom and D. Pines, Ap. J. **220**, 272 (1978).
13. P.M. Chadwick *et al.*, Nature **318**, 642 (1985).
14. For a review on pulsars see F.G. Smith, Pulsars (Cambridge: Cambridge University Press, 1977) and
J.M. Irvine, Neutron Stars (Oxford: Clarendon Press, 1978).
15. W.T. Verstrand and D. Eichler, Ap. J. 261, 251 (1982);
V.S. Berenzinsky, *Proceedings of 1979 DUMAND Summer Workshop*, edited by J.G. Learned, p. 245;
D. Eichler, Nature **275**, 725 (1978).

16. T.K. Gaisser and T. Stanev, Phys. Rev. Lett. **54**, 2265 (1985).
17. For a review on acceleration by pulsar DC electric fields, see E.T. Scharlemann, in Acceleration Mechanisms in Astrophysics, *La Jolla Institute 1979*, edited by J. Arons and C. McKee (New York: American Institute of Physics, 1979) pp. 373–390;
for the possible acceleration mechanisms in Cygnus X-3, see D. Eichler and W.T. Vestrand, Nature **307**, 613 (1984) and *Proceedings of the* 19^{th} *International Cosmic-Ray Conference*, La Jolla, 1985 (Washington D.C.: NASA, 1985);
G. Chanmugam and K. Brecher *et al.*, Nature, **313**, 767 (1985);
D. Kazanas and D.C. Ellison, Nature, to be published.
18. A.M. Hillas, Nature **312**, 50 (1984).
19. T.K. Gaisser, talk at *Telemark IV* (1987).
20. T.K. Gaisser, F.W. Stecker, A.K. Harding and J.J. Barnard, Ap. J. **309**, 674 (1986);
F.W. Stecker, A.K. Harding and J.J. Barnard, Nature **316**, 418 (1985).
21. T.K. Gaisser and F. Halzen, *XXIst Rencontre de Moriond*, Les Arcs, 1986.
22. For the results of Monte-Carlo studies on muon production by gamma-ray showers, see T. Stanev and C.P. Vankov, Phys. Lett. **158B**, 75 (1985);
T. Stanev, C.P. Vankov, and F. Halzen, in *Proceedings of the* 19^{th} *International Cosmic-Ray Conference*, La Jolla, 1985 (Washington D.C.: NASA, 1985), Vol. 7, p. 219;

and for the algorithms used in the Monte-Carlo studies, see T. Stanev and C.P. Vankov, Comp. Phys. Comm. **16**, 363 (1979).

23. T.K. Gaisser and T. Stanev, Phys. Rev. Lett. **54**, 2265 (1985);
E.W. Kolb, M.S. Turner and T.P. Walker, Phys. Rev. **D32**, 1145 (1985); **33**, 859 (1986); T.P. Walker, E.W. Kolb and M.S. Turner, in *Proceedings of New Particles '85*, Madison, Wisconsin, edited by V. Barger, D. Cline and F. Halzen (Singapore: World Scientific, 1986);
A. Dar, Phys. Lett. **159B**, 205 (1985) ;
V.S. Berezinskiĭ, C. Castagnolia and P. Galeotti, Nuovo Cimento **8C**, 185 (1985);
H. Lee and S. Bludman, Ap. J. **290**, 28 (1985).

24. V.J. Stenger, Nature **317**, 411 (1985) and Ap. J. **284**, 810 (1984);
R.W. Robinett, Phys. Rev. Lett. **55**, 469 (1985);
G. Auriemma, L. Maiani and S. Petrarca, Phys. Lett. **164B**, 179 (1985);
V.S. Berezinskiĭ, É.V. Bugaev and E.S. Zaslavskaya, JETP Lett. **42**, 528 (1985);
V.S. Berezinskiĭ, Sov. J. Nucl. Phys. **41**, 251 (1985);
B.A. Arbuzov, JETP Lett. **42**, 532 (1985);
S. Midorikawa and S. Yoshimoto, University of Tokyo preprint INS-RE.-560 (1985).
For related suggestions see A. Zee, Phys. Lett. **161B**, 141 (1985);
R.N. Mohapatra, S. Nussinov and J.W.F. Valle, Phys. Lett. **165B**, 417 (1985).

25. J.R. Cudell and F. Halzen, Madison Preprint MAD/PH/323 (1987) (to be published in Phys. Rev. D).

26. H.E. Haber and G. Kane, Phys. Rep. **117**, 279 (1983).

27. See *e.g.* S. Dawson, E. Eichten and C. Quigg, Phys. Rev. **D31**, 1581 (1985).

28. V. Barger, S. Jacobs, J. Woodside and K. Hagiwara, Phys. Rev. **D33**, 57 (1986).

29. J. Ellis, *Lake Louise Winter Institute*, CERN-TH.4391 (1986) and references therein.

30. M.L. Marshak *et al.*, Phys. Rev. Lett. **54**, 2079 (1985); **55**, 1965 (1985); G. Battistoni *et al.*, (NUSEX Collaboration), Phys. Lett. **155B**, 465 (1985).

31. M. L. Marshak, in *Proceedings of the XXIII International High-Energy Physics Conference* (Berkeley), 1986;
IMB Collaboration, Phys. Rev. D (1986), to be published.

32. T. Stanev, T.K. Gaisser and F. Halzen, Phys. Rev. **D32**, 1244 (1985).

33. K. Ruddick, Phys. Rev. Lett. **57**, 531 (1986)and references therein.

34. F. Halzen, P. Hoyer and N. Yamdagni, Madison Preprint MAD-PH-322 (1987) and references therein;
G. Domokos, S. Kövesi-Domokos and S. Nussinov, Johns Hopkins preprints JHP-HET 8603, 8605 and 8608 (1986).

35. F. Halzen, Nucl. Phys. **A461**, 181 (1987).

Table I. Signal-over-background ratio [see Eqs. (4.34.a, b)] for $E_{min} = 10$ TeV, $E_{max} = 10^5$ TeV, $T = 4.8$ hours, $\delta\phi = 0.05\ T$, $M_{C'} \approx M_C$ and $f = 1\%$.

M_C (TeV)	n	S/B	S/B in 3° cone
0.1	-1.0	6.7	6.8
0.1	-1.5	0.6	1.2
0.1	-2.0	0.05	2.1
1.0	-1.0	1.8	2.2
1.0	-1.5	0.1	3.2
1.0	-2.0	0.01	2.2

Table II. Heating of the companion star.

$m_{\tilde{g}}$ (GeV)	$m_{\tilde{q}}$ (GeV)	heating (10^{33} GeV s^{-1})
3	300	2.1×10^3
7	100	1.5×10^6
60	600	4.1×10^3

FIGURE CAPTIONS

1. Time differential flux of cygnets and average cygnet energy at Earth for a cygnet mass $m = 1$ GeV, a period $T = 4.8$ hours, a pulse width at the star $\delta\phi = 0.05\ T$, a flux normalized to 1 particle per second, an energy spread $[E_{min} = 10$ TeV, $E_{max} = 10^5$ TeV] and an energy exponent $n = -1, -2, -3$. $t = 0$ is taken to be the arrival time of the first highest-energy particles.

2.a Same as Fig. 1 for $m = 100$ GeV and $n = -1, -1.5, -2$.

2.b Same as Fig. 1 for $m = 1$ TeV and $n = -1, -1.5, -2$.

3.a $\delta\phi$ dependence of the signal and of the average cygnet energy for $m = 100$ GeV, $n = -2$, $E_{min} = 100$ TeV and $\delta\phi/T = 10\%$, 5% and 1% (the other parameters are as in Fig. 1).

3.b E_{min} dependence of the signal and of the average cygnet energy. Same parameters as in Fig. 3.a with $\delta\phi/T = 5\%$ and $E_{min} = 10$, 10^2 and 10^3 TeV.

4. Energy dependence of the photino flux at Earth for models I and II described by Eq. (4.32), compared with neutrino and photon fluxes.

5. Phase dependence of the photino fluxes at Earth for cases I and II described by Eq. (4.32). The flux vanishes between $\phi = 0.22$ and 0.78 and is the mirror image of Fig. 2 in the interval $\phi = 0.78 - 1.0$.

6. Stable-gluino fluxes at Earth compared with the results from Ref. 10.

7. Photino interaction cross sections with protons are compared with neutrino and antineutrino cross sections. These cross sections determine the absorption of flux by the companion star.

8. Time-dependent angular spread of the muon signal assuming $M_{C'} \approx M_C$ and $f = 10^{-2}$. The results are given for $M_C = 100$ GeV and 1 TeV, the other parameters being the same as in Fig. 1.

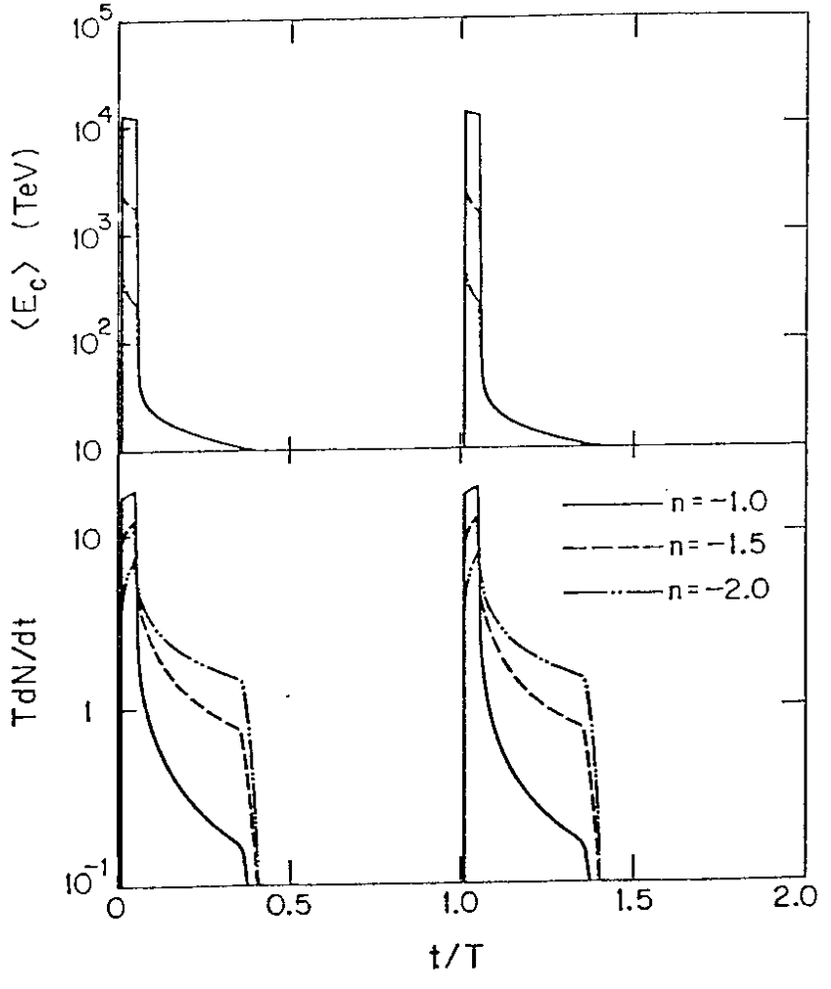

Figure 1

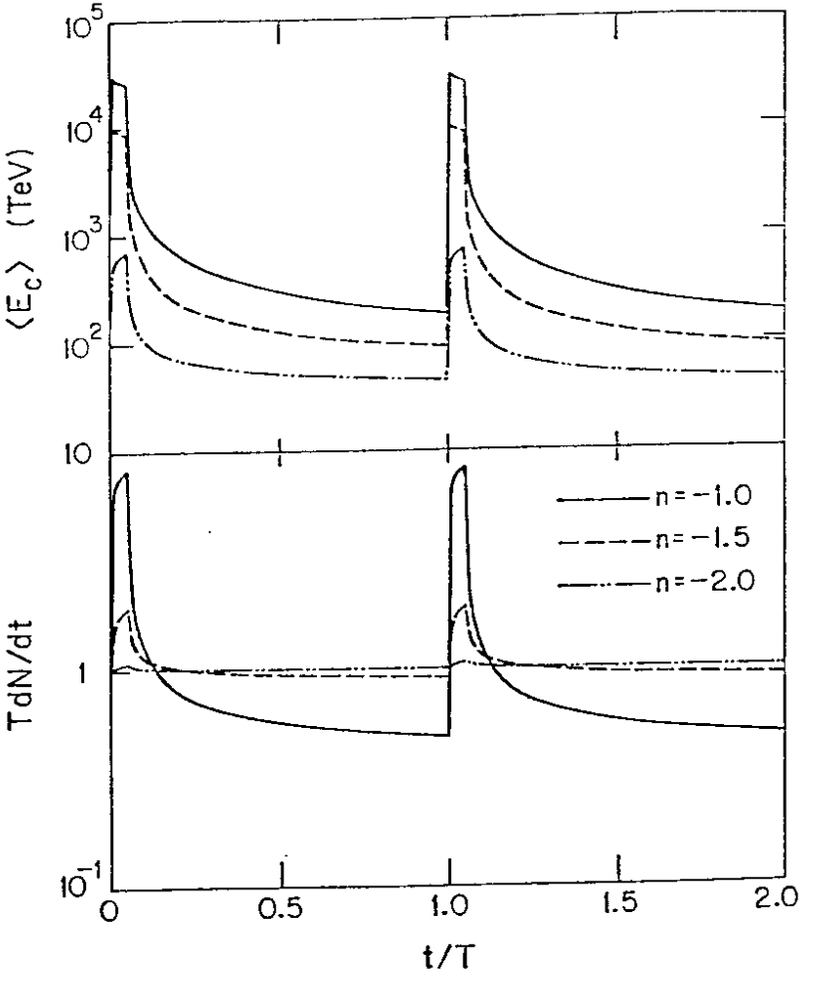

Figure 2.a

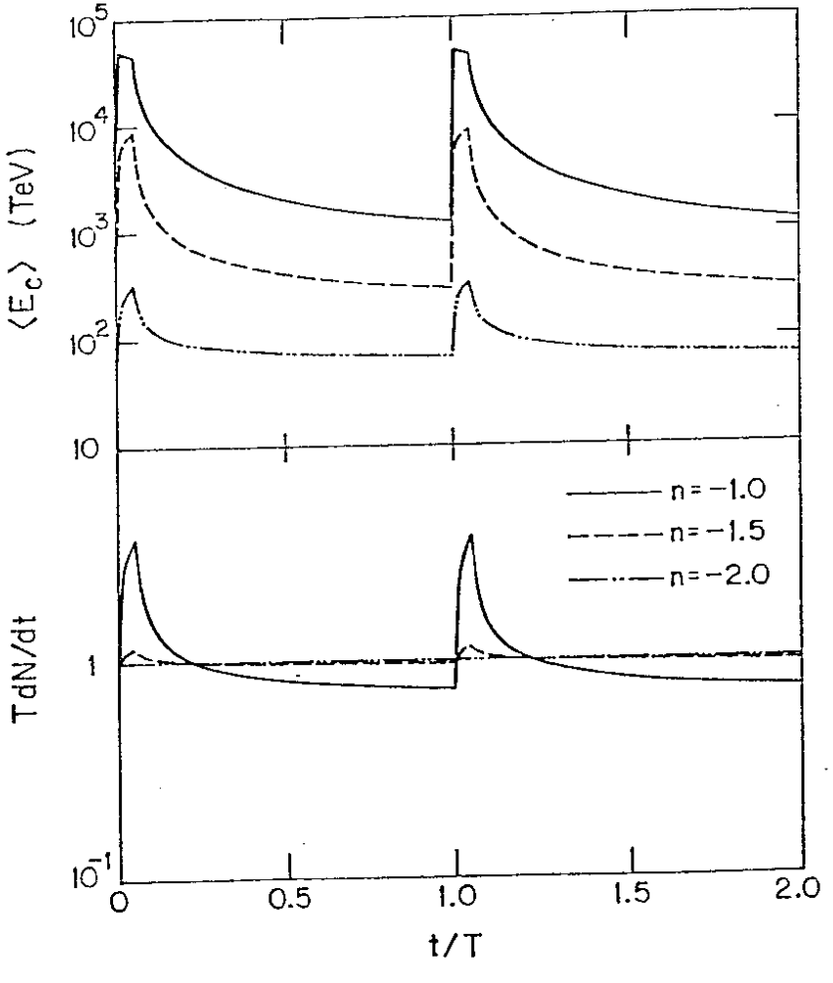

Figure 2.b

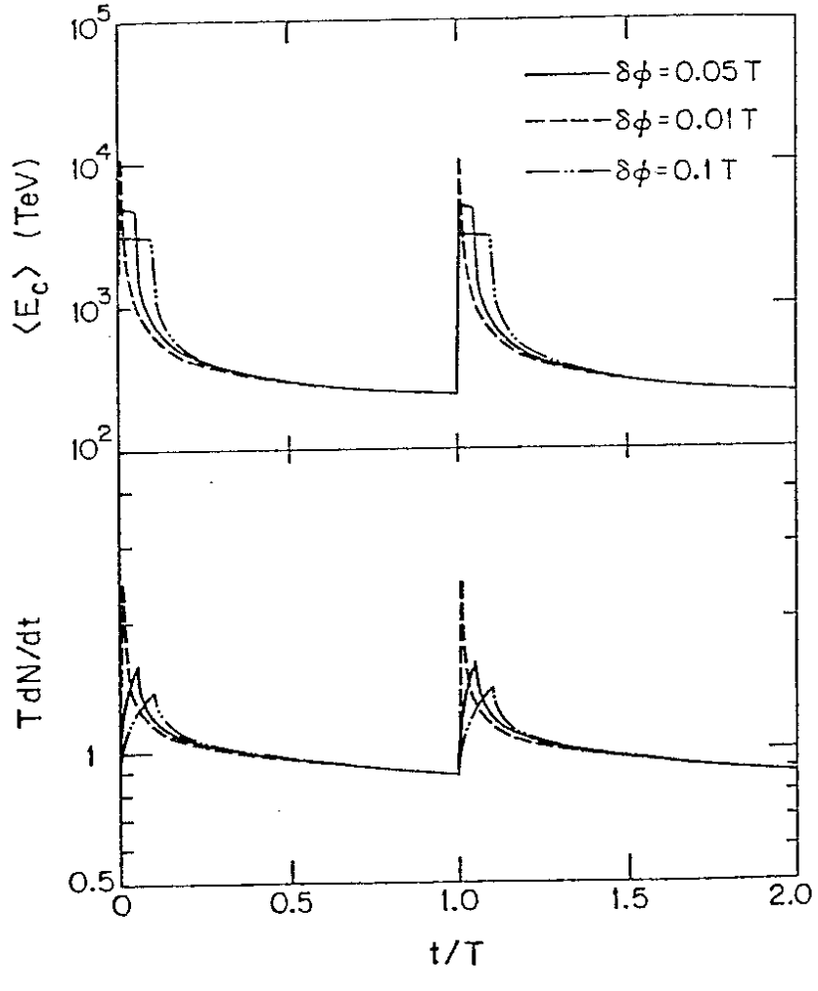

Figure 3.a

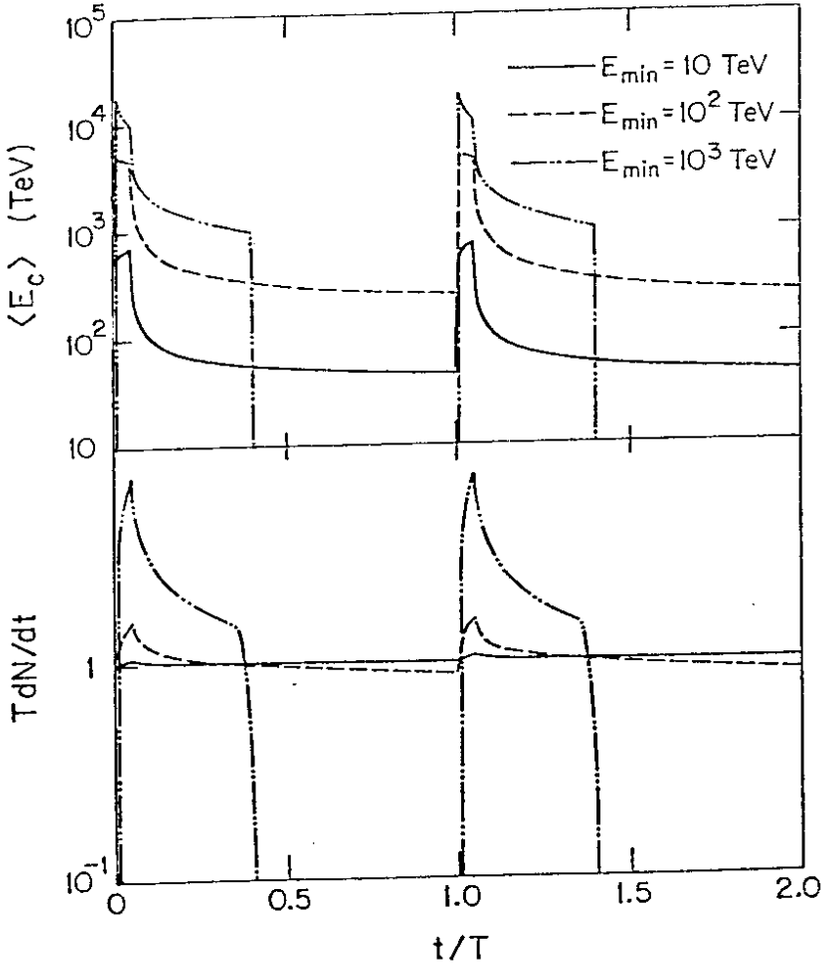

Figure 3.b

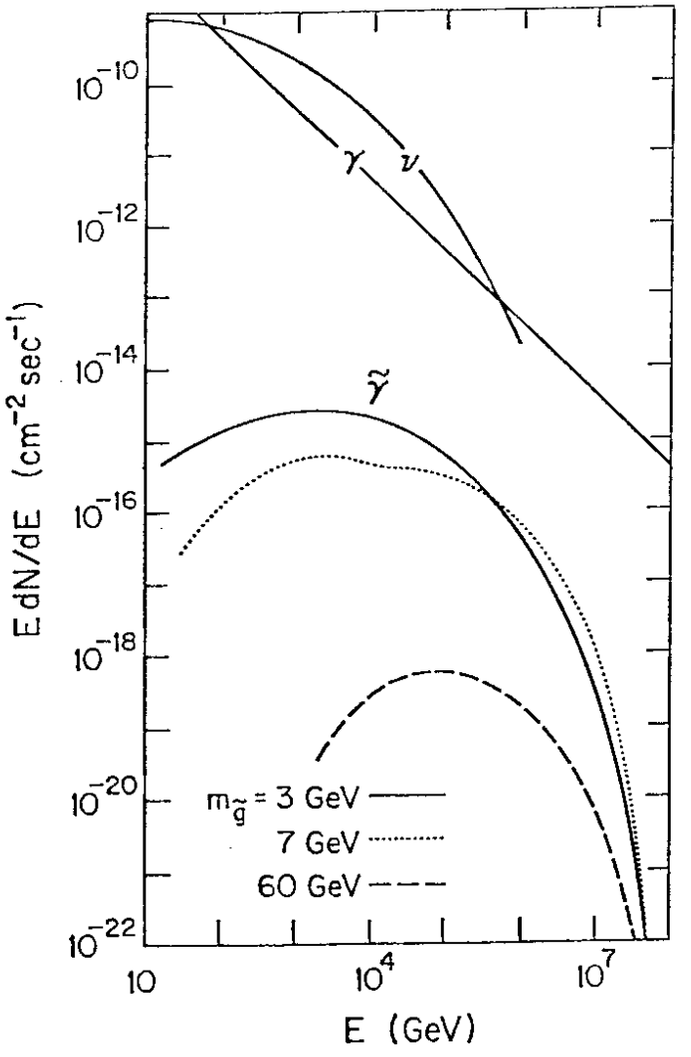

Figure 4

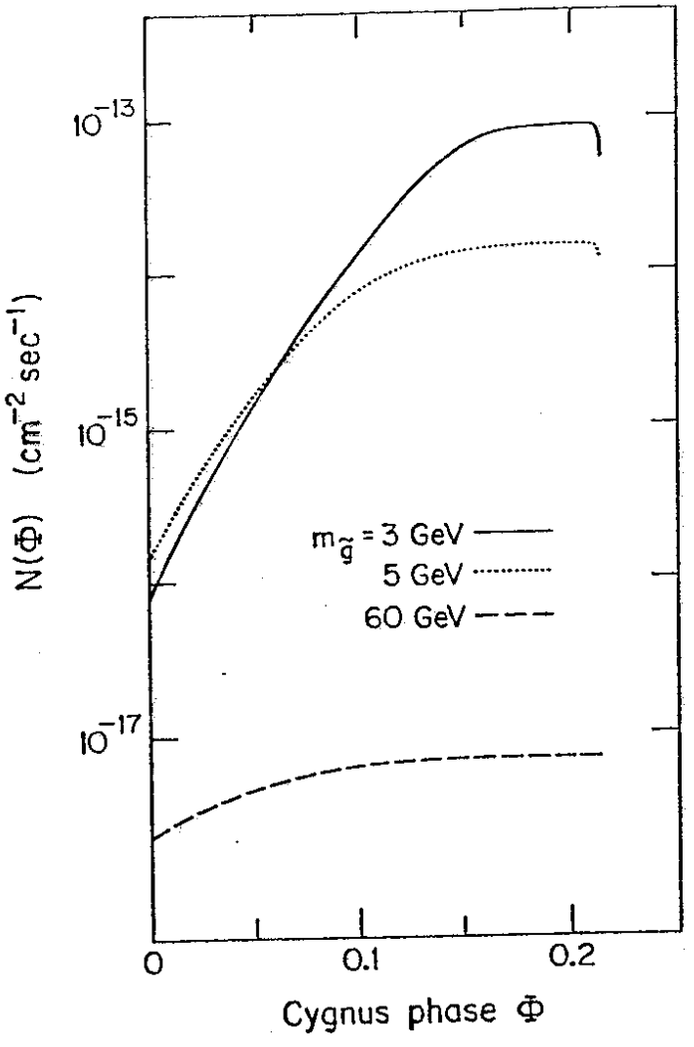

Figure 5

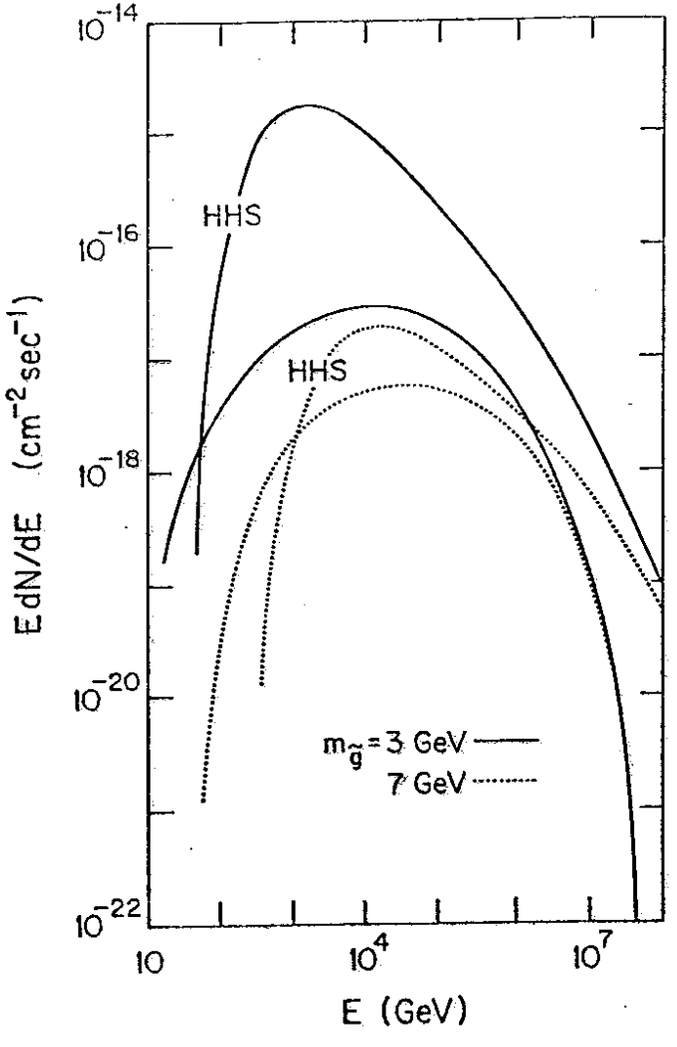

Figure 6

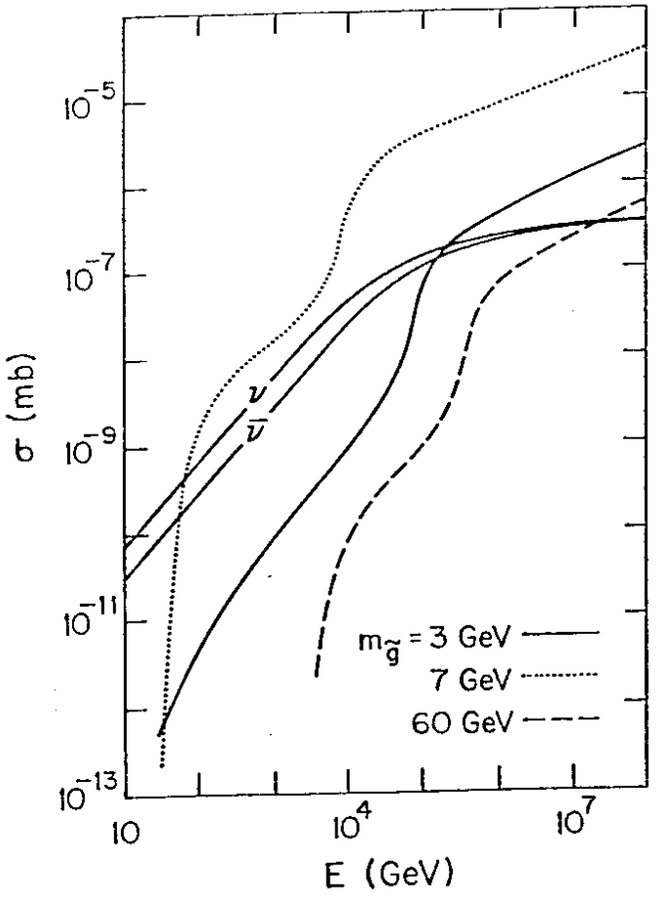

Figure 7

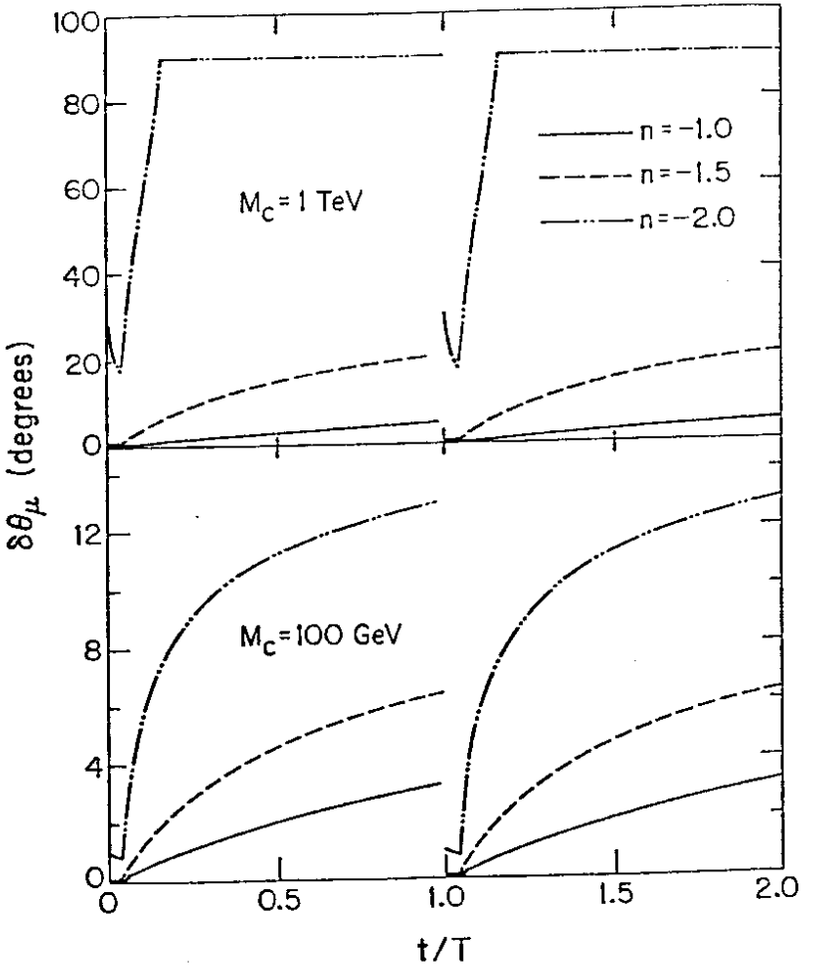

Figure 8

APPENDIX A

Kinematics of Same-Sign-Dilepton Production

The notation we are using is defined in Fig. A1. The four-particle phase space is given by:

$$dPS = \frac{d^3k'}{2k'_0}\frac{d^3p''_u}{2p''_{0u}}\frac{d^3p_c}{2E_c}\frac{d^3p_{\bar{c}}}{2E_{\bar{c}}}\delta^4(k+p-k'-p''_u-p_c-p_{\bar{c}})$$

and one can rewrite it:

$$dPS = \frac{\pi}{64}\hat{s}\ y\ \beta_c\ dy\ d\hat{x}\ d\hat{z}\ dM^2\ d\phi_g\ d\cos\theta_c\ d\phi_c$$

$$\text{with : } \beta_c = \sqrt{1-\frac{4m_c^2}{M^2}}$$

$$0 \leq \hat{x}, y \leq 1$$

$$4m_c^2 \leq M^2 \leq \hat{w}^2$$

$$\text{and } R \equiv M^2/\hat{w}^2 \leq \hat{z} \leq 1$$

In the Wd center-of-momentum frame, one has then:

$$q = \frac{\hat{w}}{2(1-\hat{x})}(1-2\hat{x},0,0,1)$$

$$p = \frac{\hat{w}}{2(1-\hat{x})}(1,0,0,-1)$$

$$k = \frac{\hat{w}}{2(1-\hat{x})y}(1-\hat{x}y, 2\sqrt{\hat{x}(1-\hat{x})(1-y)}, 0, 1-2\hat{x}+\hat{x}y)$$

$$k' = \frac{\hat{w}}{2(1-\hat{x})y}(1-y+\hat{x}y, 2\sqrt{\hat{x}(1-\hat{x})(1-y)}, 0, (1-\hat{x})(1-y)-\hat{x})$$

$$p'_g = \frac{\hat{w}}{2}(1+R, 2\sqrt{(\hat{z}-R)(1-\hat{z})}\cos\phi_g, 2\sqrt{\hat{z}-R)(1-\hat{z})}\sin\phi_g, 2\hat{z}-1-R)$$

$$p''_u = (\frac{\hat{w}}{2}(1-R), -\vec{p'_g})$$

Some of the invariants can be simply rewritten, with ξ the parton momentum fraction:

$$\hat{s} = \xi(s-m_p^2)$$

$$k\cdot p = \frac{\hat{s}}{2}$$

$$p_g\cdot p_g = M^2$$

$$p'_g\cdot p''_u = \frac{1}{2}(\hat{w}^2-M^2)$$

$$p'_g\cdot p = \frac{1}{2}y\hat{z}\hat{s}$$

$$k\cdot k' = \frac{1}{2}\hat{s}\hat{x}y$$

$$p\cdot p''_u = \frac{1}{2}\hat{s}y(1-\hat{z})$$

$$p\cdot k' = \frac{\hat{s}}{2}(1-y)$$

and the muon energy is:

$$E_\mu = \frac{(s-m_p^2)(1-y)}{m_p}$$

In the gluon rest frame, the charm-quark momentum can be written:

$$c^* = \frac{M}{2}(1, \beta_c\cos\theta_c\ \cos\phi_c, \beta_c\sin\theta_c\sin\phi_c, \beta_c\cos\theta_c)$$

$$\bar{c}^* = \frac{M}{2}(1, -\vec{p_c})$$

and these need to be boosted to the Wd rest frame. Taking the third axis along the gluon direction gives a boost:

$$p_{c0} = \frac{g_0 c_3^* + \tilde{g} c_0^*}{M_g}$$

$$p_{c1} = \frac{(g_0 c_3^* + g c_0^*) g_1}{g M_g} - \frac{c_2^* g_1 g_3}{g g_T} - \frac{c_1^* g_2}{g_T}$$

$$p_{c2} = \frac{(g_0 c_3^* + g c_0^*) g_2}{g M_g} - \frac{c_2^* g_2 g_3}{g g_T} + \frac{c_1^* g_1}{g_T}$$

$$p_{c3} = \frac{(g_0 c_3^* + g c_0^*) g_3}{g M_g} + \frac{c_2^* g_T}{g}$$

with $g_\alpha \equiv (p_g)_\alpha$, $M_g = \sqrt{g_0^2 + g_1^2 + g_2^2 + g_3^2}$, $g = \sqrt{g_1^2 + g_2^2 + g_3^2}$ and $g_T = \sqrt{g_1^2 + g_2^2}$.

FIGURE CAPTION

A1. Notation used in the kinematics of same-sign-dilepton production. The letters in parenthesis label the particle 4-momentum and the arrows indicate the chosen sign convention.

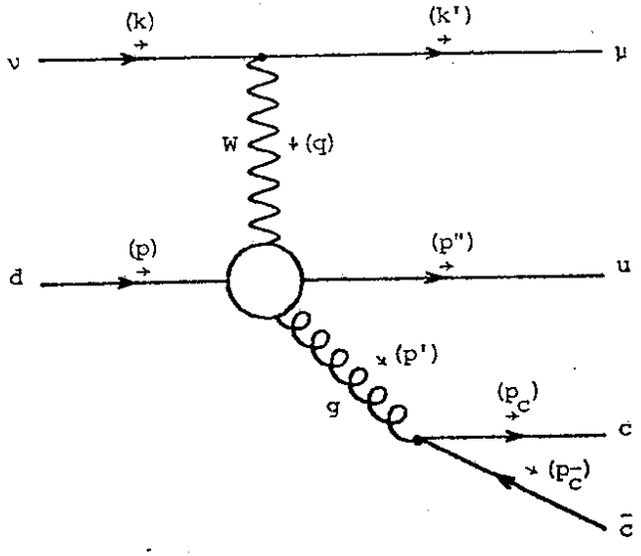

Figure A1

APPENDIX B

Photino Interaction Cross Section

The elementary interaction cross section for the process $\tilde{\gamma} + q \rightarrow \tilde{g} + q$ (see Fig. B1), taking fully into account the squark propagator, is given by:

$$\frac{d\hat{\sigma}}{d\hat{x}} = (C_1 + C_4)(\hat{s} - m_{\tilde{\gamma}}^2 - m_{\tilde{g}}^2 + \frac{m_{\tilde{g}}^2\, m_{\tilde{\gamma}}^2}{\hat{s}}) + (\frac{C_3}{\Gamma_{\tilde{q}}} - C_1\, \Gamma_{\tilde{q}}) \arctan(T) + \frac{C_2}{2} \log(E)$$

where:

$\Gamma_{\tilde{q}}$ is the squark width times the squark mass, given by (for $m_{\tilde{\gamma}} \approx 0$):

$$\Gamma_{\tilde{q}} = \frac{4}{3}\alpha_S \frac{(m_{\tilde{q}}^2 - m_{\tilde{g}}^2 - m_q^2)}{m_{\tilde{q}}}\, \lambda^{1/2}(m_{\tilde{q}}^2, m_{\tilde{g}}^2, m_q^2)$$
$$+ e_q^2\, \alpha\, \frac{(m_{\tilde{q}}^2 - m_q^2)}{m_{\tilde{q}}} \lambda^{1/2}(m_{\tilde{q}}^2, 0, m_q^2)$$

the coefficients C_i are found to be:

$$C_1 = 1 + 2\, m_{\tilde{g}}\, m_{\tilde{\gamma}}\, \frac{\hat{s} - m_{\tilde{g}}^2}{(\hat{s} - m_{\tilde{q}}^2)^2 + \Gamma_{\tilde{q}}^2}$$

$$C_2 = 2\, m_{\tilde{q}}^2 - m_{\tilde{\gamma}}^2 - m_{\tilde{g}}^2 + 2\, m_{\tilde{g}}\, m_{\tilde{\gamma}}\, \frac{(\hat{s} + m_{\tilde{q}}^2 - m_{\tilde{\gamma}}^2 - m_{\tilde{g}}^2)(\hat{s} - m_{\tilde{q}}^2) + \Gamma_{\tilde{q}}^2}{(\hat{s} - m_{\tilde{q}}^2)^2 + \Gamma_{\tilde{q}}^2}$$

$$C_3 = (m_{\tilde{q}}^2 - m_{\tilde{g}}^2)(m_{\tilde{q}}^2 - m_{\tilde{\gamma}}^2) + 2\, m_{\tilde{g}} m_{\tilde{\gamma}} \frac{(\hat{s} + m_{\tilde{q}}^2 - m_{\tilde{g}}^2 - m_{\tilde{\gamma}}^2)\Gamma_{\tilde{q}}^2}{(\hat{s} - m_{\tilde{q}}^2)^2 + \Gamma_{\tilde{q}}^2}$$

$$C_4 = \frac{(\hat{s} - m_{\tilde{\gamma}}^2)(\hat{s} - m_{\tilde{g}}^2)}{(\hat{s} - m_{\tilde{q}}^2)^2 + \Gamma_{\tilde{q}}^2}$$

and the arguments of the tangent and of the logarithm are:

$$T = \frac{(\hat{s} - m_{\tilde{g}}^2 - m_{\tilde{\gamma}}^2 + \frac{m_{\tilde{g}}^2 m_{\tilde{\gamma}}^2}{\hat{s}})\Gamma_{\tilde{q}}}{\Gamma_{\tilde{q}}^2 + (m_{\tilde{q}}^2 - \frac{m_{\tilde{g}}^2 m_{\tilde{\gamma}}^2}{\hat{s}})(m_{\tilde{q}}^2 + \hat{s} - m_{\tilde{g}}^2 - m_{\tilde{\gamma}}^2)}$$

$$E = \frac{(m_{\tilde{q}}^2 - \frac{m_{\tilde{g}}^2 m_{\tilde{\gamma}}^2}{\hat{s}})^2 + \Gamma_{\tilde{q}}^2}{(m_{\tilde{g}}^2 - m_{\tilde{q}}^2 + m_{\tilde{\gamma}}^2 - \hat{s})^2 + \Gamma_{\tilde{q}}^2}$$

FIGURE CAPTION

B1. Leading-order Feynman diagrams for photino-quark interactions.

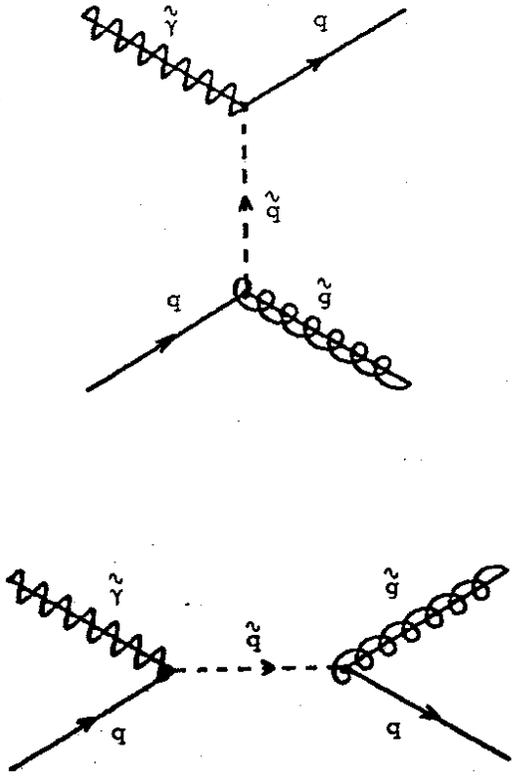

Figure B1